JTTEE5 19:56–80
DOI: 10.1007/s11666-009-9435-x
1059-9630/$19.00 © ASM International

From Powders to Thermally Sprayed Coatings

Pierre Fauchais, Ghislain Montavon, and Ghislaine Bertrand

(Submitted April 23, 2009; in revised form September 30, 2009)

Since the early stages of thermal spray, it has been recognized that the powder composition, size distribution, shape, mass density, mechanical resistance, components distribution for composite particles play a key role in coating microstructure and thermo mechanical properties. The principal characteristics of particles are strongly linked to the manufacturing process. Coatings also depend on the process used to spray particles and spray parameters. Many papers have been devoted to the relationships existing between coating properties and structures at different scales and manufacturing processes. In many conventional spray conditions resulting in micrometric structures, among the different parameters, good powder flow ability, and dense particles are important features. Thermal plasma treatment, especially by RF plasma, of particles, prepared by different manufacturing processes, allows achieving such properties and it is now developed at an industrial scale. Advantages and drawbacks of this process will be discussed. Another point, which will be approached, is the self-propagating high-temperature synthesis, depending very strongly upon the starting composite particle manufacturing. However, as everybody knows, "small is beautiful" and nano- or finely structured coatings are now extensively studied with spraying of: (i) very complex alloys containing multiple elements which exhibit a glass forming capability when cooled-down, their under-cooling temperature being below the glass transition temperature; (ii) conventional micrometer-sized particles (in the 30-90 μm range) made of agglomerated nanometer-sized particles; (iii) sub-micrometer- or nanometer-sized particles via a suspension in which also, instead of particles, stable sol of nanometer-sized particles can be introduced; and (iv) spray solutions of final material precursor. These different processes using plasma, HVOF or sometimes flame and also cold-gas spray will be discussed together with the production of nanometer-sized particles via the chemical reaction method or by a special type of milling: the cryogenic milling process often referred to as "cryomilling."

Keywords coating, cold-gas spraying, feedstock, manufacturing routes, nanometer-sized particle, thermal spray processes

1. Introduction

The structure and properties of coatings manufactured by thermal or cold-gas spraying depend strongly upon powder feedstock morphologies, injection of feedstock into the energetic flow, and spray operating conditions (Ref 1-4). Indeed, the powder feedstock morphology and particles size distribution are related to its manufacturing route. Since about a decade many works have been devoted to nanometer-sized structured coatings for which nanometer-sized particles or particles susceptible to form nanometer-sized structures upon cooling are developed. The injection of these particles into the energetic gas flow and the resulting trajectories condition distributions at impact of particle velocities, temperatures, indexes of melting (except for cold spray) and chemical reactions with the particles surrounding atmosphere or within. The spray operating conditions, including the spray distance, control the substrate and coating temperatures (preheating, spraying, and coating cooling), the deposited spray pattern, the residual stress distribution and its possible relaxation, etc.

This paper aims at reviewing our present knowledge in this field. First the major powder manufacturing technologies are summarily presented and a few processes are emphasized. The influence of the particles treatment in-flight is then described. On the one hand, particles injection plays a key role, together with their morphology, on their heating and acceleration. On the other hand, chemical reactions with the surrounding atmosphere and/or solid reactions (SHS type, self-propagating high-temperature

This article is an invited paper selected from presentations at the 2009 International Thermal Spray Conference and has been expanded from the original presentation. It is simultaneously published in *Expanding Thermal Spray Performance to New Markets and Applications: Proceedings of the 2009 International Thermal Spray Conference*, Las Vegas, Nevada, USA, May 4-7, 2009, Basil R. Marple, Margaret M. Hyland, Yuk-Chiu Lau, Chang-Jiu Li, Rogerio S. Lima, and Ghislain Montavon, Ed., ASM International, Materials Park, OH, 2009.

Pierre Fauchais and **Ghislain Montavon**, SPCTS—UMR CNRS 6638, Faculty of Sciences and Technologies, University of Limoges, 123 Avenue Albert Thomas, 87060 Limoges cedex, France; and **Ghislaine Bertrand**, LERMPS—EA 3316, University of Technology of Belfort-Montbéliard, site de Sévenans, 90010 Belfort cedex, France. Contact e-mails: fauchais@unilim.fr and ghislain.montavon@unilim.fr.

synthesis) within particles can occur. The issues associated to coating building mechanisms including the influence of spray conditions on splat formation and layering are also described. Out of the scope of this review are the liquid and gas precursors.

2. Powders

2.1 Introduction

Powders with identical chemical composition and size distribution from various suppliers can have very different morphologies owing to the powder manufacturing routes used. Thus, thermally sprayed coatings can exhibit in such a case significant structural variations (Ref 5). This has been demonstrated for plasma spraying (Ref 6-11), high-velocity oxy-fuel (HVOF) (Ref 12-16), D-gun (Ref 17), and pulsed gas dynamic spraying process (Ref 18). The powder morphology, resulting from their manufacturing process, varies from spherical to irregular or blocky (Ref 1). Irregular shapes range from cubic-like structures to needles with high-elongation ratio whereas blocky particles usually exhibit an elongation ratio close to unity. Moreover, if blocky particles are always dense, spherical and irregular ones can be dense or porous with a rather wide range of void content (Ref 2-4). Beside the effect of particle shape on their aerodynamic behavior, different particle-specific masses (corresponding to particles with different void contents) result in different thermal conductivities and diffusivities and thus in different particle heat treatments.

The flowability of powders (i.e., their capability in flowing through the powder feeder and injection system, usually measured by Hall flowmeter) is extremely important in all thermal spray processes. Poor flowability results in fluctuations in powder feed rate and thus in inhomogeneous coating structures.

The powder mass flow rate also depends directly upon its specific mass (Ref 19), which is the highest for dense spherical particles such as those densified by RF plasmas (Ref 20).

Morphology is also a key parameter for particle behavior upon penetration within the plasma jet (Ref 21), for example, since de-agglomeration of agglomerated and partially calcinated particles can occur.

The homogeneity of particles composition (Ref 6, 8) is another key parameter for coating behavior, especially at high temperatures. For example partially yttria (8 wt.%) stabilized zirconia fused and crushed (FC) particles keep their tetragonal nontransformable structure up to about 1300 °C, while those prepared by sol-gel process can be heated up to 1400 °C before transformation occurs (Ref 22). This is due to the more homogeneous distribution of yttria in the zirconia super-lattice resulting from sol-gel technique. For complex coatings, such as quasi-crystalline ones (Ref 23, 24), or mullite ones (Ref 25), there is also a close correlation between powder manufacturing route, phase structure, crystallinity, and coating properties.

The oxidation level of particles during their manufacturing process is also a very important issue to be considered because obviously the oxide content in coatings is never lower than that of sprayed particles.

Finally, it must be kept in mind that powder characterization is not necessarily straightforward. For example, the characterization of particle size distribution (Ref 26) may vary depending upon the particle morphology.

2.2 Atomized Powders

Atomization is a very common route to manufacture metal and alloy powders (Ref 1). In this process, a molten metal flow is atomized into droplets which are rapidly solidified before their impact onto the manufacturing chamber or their agglomeration/coalescence. The starting material, in the form of elemental or multielemental metallic alloys, is melted in an induction, arc, or other type of furnace. After the starting material is molten and the resulting bath made homogenous, it is transferred to a tundish which aims at supplying a constant, controlled flow of metal into the atomizing chamber. The stream exiting the tundish is intercepted by the high velocity stream of the atomizing medium (water, air, or inert gas) atomizing it into fine droplets. For particles collected in the lower part of the atomizing chamber, the two important issues are on the one hand their size distribution and shape (if possible with a high degree of sphericity) and on the other one their degree of oxidation. In fact sphericity is also correlated to the particle oxidation in-flight (Ref 27). Oxidation is important when atomization is performed with water and much less with neutral gases (generally argon or nitrogen), but it becomes a rather expensive manufacturing process in this later case.

In the past decade, a series of new bulk amorphous alloys with a multicomponent chemistry and high glass forming ability (GFA) have been developed in zirconium-, magnesium-, lanthanum-, palladium-, titanium-, and Fe-base systems with various rapid solidification techniques (Ref 28). Compared with other amorphous alloy systems, in particular zirconium- and lead-base metallic glasses, the advantages of Fe-base amorphous coatings are lower materials cost, higher strength, and higher wear and corrosion resistances. For example, to manufacture amorphous and nanometer-sized composite thermally deposited steel coatings, a specialized iron-based composition (Ref 29, 30) ($Fe_{63}Cr_8Mo_2B_{17}C_5Si_1Al_4$) with a low critical cooling rate (10^4 K s^{-1}) for metallic glass formation has been developed. The alloy is processed by inert gas atomization to form micrometer-sized amorphous spherical particles with a size distribution adapted to thermal spraying, and then sprayed to form coatings. Since the mid-eighties, a few studies have been devoted also to the production and properties of HVOF sprayed amorphous/nanometer-sized crystalline NiCrB- and FeCrB-based alloys (Ref 31).

For those materials, in-flight particle oxidation must be avoided to the maximum possible extend because oxidation triggers the destabilization of the bulk metallic glass particle: amorphous phase stability and formability are

hence largely affected by the chemical composition dependent critical cooling rate. Thus, inert gas atomization is mandatory to produce sprayable particles.

2.3 Fused and Crushed Powders

Fusing and crushing technique is devoted to brittle materials, mainly ceramics. The different components of the powder (for example, zirconia and yttria) are mixed and melted in special furnaces. After cooling, the ceramic resulting block is crushed by various ways such as hammer mills, stamping mills, jaw crushers, and gyratory crushers (Ref 27). Resulting powder particles are dense, blocky, and angular.

2.4 Milled and Sintered Powders

Grinding generates small particles (average diameter usually smaller than 5 μm) which size is not suitable for spraying. Those small particles can be compacted (one-direction compaction), with or without a binder, and then sintered. Sintering temperature, below the melting one, must be sufficiently high to allow particles binding by chemical diffusion between them (Ref 1, 2). However, if densification increases with sintering temperature, particle grain size grows correlatively over a certain temperature (Ref 32). The resulting cake is then crushed to achieve a size distribution suitable for thermal spraying. Crushing of such sintered cakes is easier than that of fused blocks. When increasing the compaction pressure, sintering time, and temperature, the void content of the resulting particles is reduced (Ref 32). Particles are blocky and angular and more or less porous. Many carbide-metal or alloy particles are produced by this route.

2.5 Milled Powders

Milling is used to manufacture powders from the processing of brittle materials such as ceramics. When alloys and cermets are considered, the milling operation is called mechanical alloying (MA).

The most common method to reduce the ceramic particle sizes and eliminate aggregates is ball milling (Ref 1, 2, 33). A ball mill is a barrel partially filled with a grinding medium (called media) that rotates on its. Milled particle mean size can be as low as 1 μm, but impurities (debris) from the media can be embedded in the powder particles.

Thermally sprayed coatings containing solid lubricants such as graphite, PTFE, MoS_2, MnS, WS_2, CaF_2, etc. reduce the energy loss by friction and weight loss by wear (Ref 34). However these materials are difficult, if not impossible, to thermal spray because they decompose easily when over heated and corresponding particle shapes, often close to platelets, have very poor flow ability. Thus in most cases, these particles are blended in a certain mass ratio with metal particles and ball milled for a few hours, leading to the powders with either sizes below a few micrometers (Ref 35) or in the few tens of micrometers, according to the milling conditions (Ref 36). Of course, the small particles must then be granulated with some organic binders into a spherical particle of about 45 μm by spray-drying method (Ref 35) and eventually sintered before spraying.

Attrition milling differs from conventional ball milling in that the slurry containing the particles and media is stirred continuously at frequencies of 1-10 Hz. The media consists of small spheres (0.2-5 mm) that represent between 60% and 90% of the available mill volume. To limit agglomeration, organic additives are added in the slurry and typical mean particle sizes are between 0.1 and 5 μm. Camerucci and Cavalieri (Ref 37) have studied attrition milling conditions to obtain submicron particle sizes.

Cooling of the milling media and powders is an effective way to fasten the fracture processes and rapidly attain steady-state conditions (Ref 38). Cryomilling allows suppressing powder agglomeration and welding to the milling media, reducing oxidation reactions under the protection of a nitrogen environment, reducing the milling time required attaining a nanostructure. Low temperature suppresses hence the annihilation of dislocations and the accumulation of a higher dislocation density is possible.

Self-propagating high-temperature synthesis (SHS) particles represent great interest to spray (Ref 39). SHS is a highly exothermic interaction of chemical elements (or compounds) in a condensed phase that occurs in combustion conditions when heated over a critical temperature. In thermal spraying when this temperature is reached the reaction occurs in the periphery of the particle, heated by hot gases along its trajectory, and propagates toward its center. However, one of the main problems to be solved is powder preparation: when mixing intimately the reactive powders the heat generated during the powder preparation must be sufficiently low to avoid triggering the reaction. Cryomilling seems to be a promising technique for such materials.

2.6 Mechanical Alloying and Milling

Mechanical alloying is a solid-state powder processing technique involving repeated welding, fracturing, and re-welding of powder particles in a high-energy ball mill as detailed in the review paper of Suryanarayana (Ref 40). MA is a complex process and hence involves optimization of a number of variables to achieve the desired product phase and/or microstructure. Significant quantities of nanometer-structured materials with a grain size in the range of 10-200 nm are processed commercially using MA, which involves the transformation of plasticity-induced dislocation structures into high angle grain boundaries in metallic powders. Powders used in spray processes are produced with high-energy cryomilling attritors, working either with liquid (ethanol, methanol, liquid nitrogen, etc.) or argon atmospheres. The extremely low milling temperature in cryomilling (liquid nitrogen) suppresses the recovery and recrystallization and leads to finer grain structures and more rapid grain refinement (Ref 38). For each material, there is a minimum grain size that is obtainable by milling. This size is related to the intrinsic properties of the material, such as crystal structure. The minimum grain size seems in a first approximation to be inversely proportional to the melting

temperature or bulk modulus. It is also demonstrated (Ref 38) that cryomilling can be effectively used to manufacture ceramic reinforced metals, in which the size of the reinforcement phase can be modified, depending upon the milling parameters.

For example, commercially available atomized Al 5083 alloy powder (4.4 Mg, 0.7Mn, 0.15Cr, bal. Al (wt.%)) with a particle size lower than 45 μm was cryomilled by Ajdelsztajn et al. (Ref 41). Figure 1 presents both the as-received atomized (spherical with a large size distribution centered on 58 μm) and cryomilled (irregular and rock shaped with a narrow size distribution centered on 28 μm) Al 5083 powder.

A similar result is obtained with cryomilled NiCrAlY particles, initially spherical, formed of irregular and flake-shaped agglomerates (Ref 42). This morphology results from the continuous welding and fracturing of the powder particles during the mechanical milling process. The agglomerate average size of as-received and cryomilled powders are 28.7 and 106.0 μm, respectively. The cold-welding seems to overcome the fracture process, resulting in an increase in agglomerate sizes. The formation of the nanometer-sized crystalline structure during cryomilling is considered to be a consequence of plastic deformation at high strain rates (Ref 42). The grain size is in the nanometer range (lower than 50 nm). The increase in oxygen (0.027-0.17 wt.%) and nitrogen (0.0048-0.26 wt.%) concentrations is believed to be a consequence of the incorporation of these elements from air and liquid nitrogen environments, respectively.

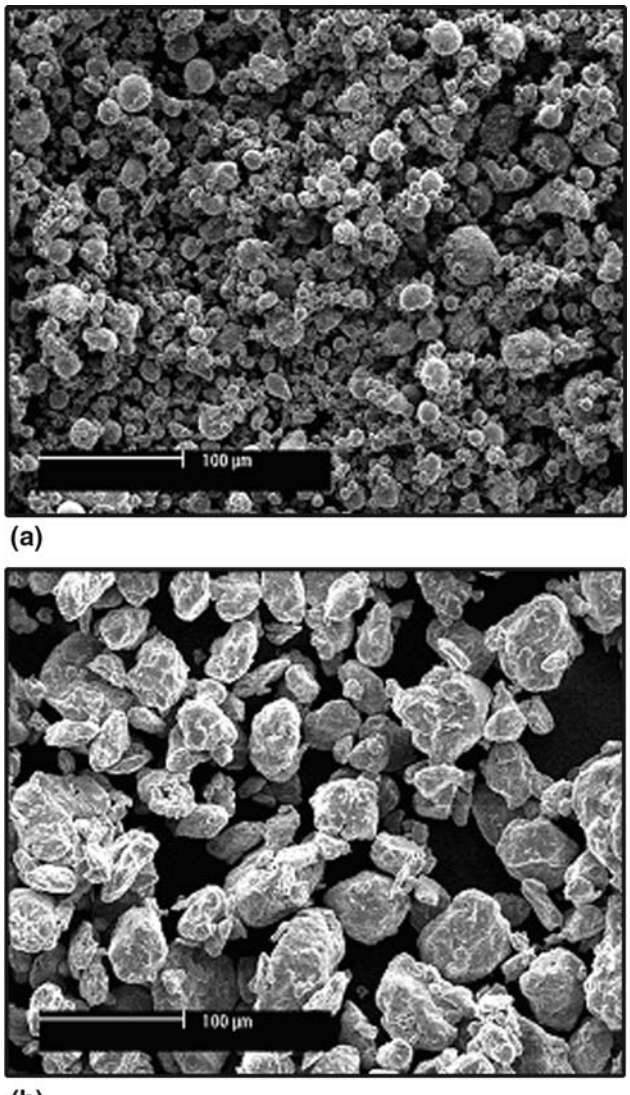

Fig. 1 Morphology of (a) as-received and (b) cryomilled Al 5083 powder (Ref 41)

The two previous cases particles (Ref 41, 42) result from metallurgical agglomeration, which is formed by cold welding. It is not anymore the case when mixtures of brittle and ductile particles where binder-induced agglomerates are primarily bonded by milling environment and can be decomposed back to their original powder form (Ref 43, 44). Here, the obtained particles are smaller than the starting ones contrary to the previously described cases. For example Cr_3C_2-25(Ni20Cr) powder was milled in hexane [$H_3C(CH_2)4CH_3$]. After 16 h of milling, the pure carbide particles were not observed. In the milled powder, the ductile (soft) Ni-rich phase is no longer seen as spherical particles, but is distributed among the homogeneous, finer particles. X-ray mapping results reveal the particles to be neither pure carbide nor pure NiCr phase (Ref 43).

TiC-Ni based nanocrystalline cermet powders, with fine, homogeneously distributed sub-micrometer-sized hard phases of TiC, have been produced by high-energy ball milling with an industrial-like vibration mill as well as with an attrition mill. It should be noted that at least 95% of the hard phase particles are smaller than 300 nm. Milling of the investigated composite material leads to a uniform particle size of 20 μm (Ref 45).

2.7 Spray-Drying

In all processes implemented to manufacture ceramic powders, the resulting size distribution is generally not adapted to that requested for spraying. Very often, and especially with crushing, grinding, milling, etc., many fine particles (below 5 μm average diameter) are produced, which are not usable for conventional spraying without agglomerating them. Beside to produce cermet particles, it is necessary to mix rather fine ceramic and metal or alloy particles and form granules of their mixtures.

Spray-drying technique is one of the most versatile ones to manufacture particles usable in spray processes from small diameter particles. In spray-drying, agglomerated powders are produced from suspensions (often water-based) called slurry. It must be noted that the formation of a stable suspension containing metal and ceramic particles is not straightforward. If the oxide suspensions are rather easy to stabilize, it is more difficult with a cermet such as WC-Co. This is due to the high-specific density of WC-Co powders and the widely different acid/base properties (i.e., zeta potential) of the two main particle constituents (Ref 46). For example in the WC-Co spray-dried powder,

the microstructure of powder is determined by micrometer-sized hard phases similar to commercial cermet feedstock, but their dispersion in the particles is not uniform (Ref 47). Fine droplets of suspension are atomized into a drying chamber where they are heated by a stream of hot air or by the radiation of the hot chamber wall or both in some cases. The rapid heat and mass transfers which occur during drying combined with the presence of various slurry compounds result in dried granules. These granules present large shape varieties: uniform solid spheres, elongated spheres, pancake shaped, donut shaped, needle-like, or hollow granules (Ref 48). In order to keep quasi-spherical shapes, particles are sintered in rotating furnaces where diffusion occurs within particles but not between themselves. In some other cases, particles are only calcinated; i.e., fired or heated at a temperature high enough to eliminate volatile constituents (which could induce otherwise the de-agglomeration of particles upon penetration in the hot gas spray stream). However, calcinated particles generally result in poor quality coatings (structural heterogeneity, large size distribution of voids, etc.).

Bertrand et al. (Ref 49) have studied the spray-drying process of ceramic powders. They have identified at least three types of resulting particles: thin-walled fractured, thin wall dimple, and thick-wall spherical depending upon the spray-drying conditions. They emphasized the importance of the slurry properties that were changed by varying the pH value, the amount of added dispersant, and the type of binder used and the solid content. The slurry formulation allows producing hollow-dried spheres or solid-dried granules.

Spray drying is also used to produce micrometer-sized particles made of individual nanometer-sized particles of generally oxides either pure or mixed (Ref 50), as illustrated in Fig. 2 (Ref 51). These agglomerated particles can be either dense, as that shown in Fig. 2, or rather porous as the ones presented in Fig. 3 (Ref 52).

This technique also allows manufacturing powders made of very dissimilar elements. For example agglomerates of particles of aluminum-silicon (Al-Si) eutectic alloy ($d_{50} = 2.4 \pm 1.2$ μm, Al-11.6 wt.% Si-0.14 wt.% Fe) in which multiwalled carbon nanotubes (CNT) (purity higher than 95%, diameter = 40-70 nm, length = 1-3 μm) are dispersed by spray drying (Ref 53). The spray-dried powders contained 5 wt.% CNT. Resulting micrometer-sized particles are displayed in Fig. 4.

2.8 Cladding

Cladding allows producing composite material particles. With this technique, particles exhibit a core of one material and an outer shell made of either a dense and continuous layer or a porous one or a heterogeneous one. Lugscheider et al. (Ref 54) have presented a very complete overview of the different cladding processes. Cladding can be used to manufacture particles where a SHS reaction can occur. This is for example the case for NiAl particles with aluminum core clad with a nickel layer. In the following, two cladding examples will be presented: mechanofusion and clad composite.

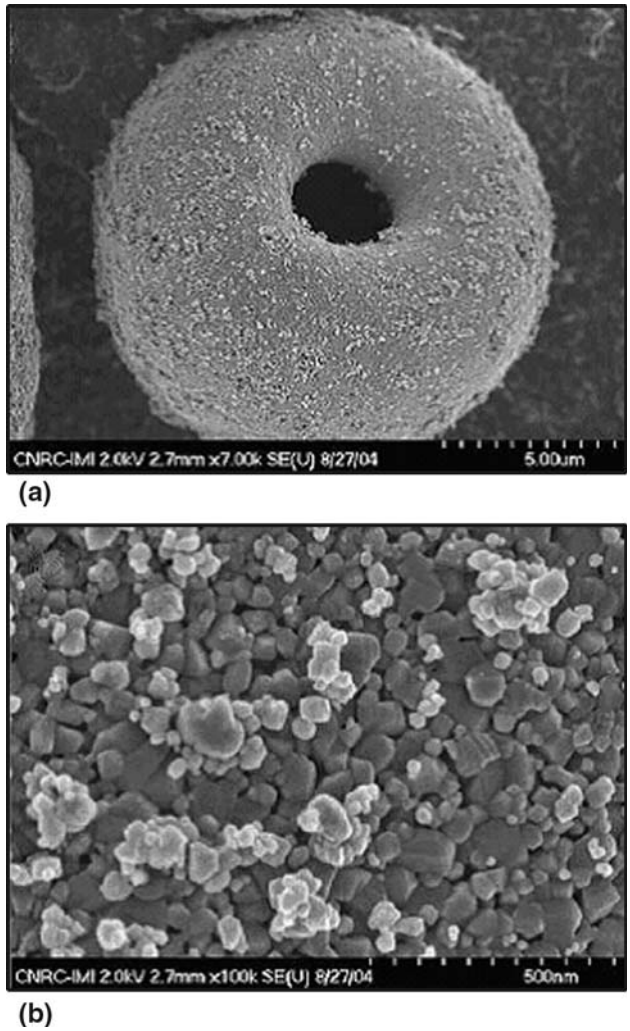

Fig. 2 (a) Titania feedstock particle formed by the agglomeration (spray-drying) of individual nanometer-sized particles. (b) Particle depicted in (a) observed at higher magnification showing individual nanometer-sized titania particles smaller than 100 nm (Ref 51)

Mechanofusion is used to manufacture composite powders starting from two or more raw powdered materials having different particles sizes (Ref 55). The raw particles are mixed intensively and subjected to a powerful compression, resulting in various types of high magnitude mechanical forces generating thermal energy. Thereby, the material with the lowest melting temperature is heated to a plastic state (or even melted in some cases) and becomes the core of a composite particle to which the material with the highest melting temperature is welded as a surrounding shell. For example (Ref 56), when starting from pure α-alumina (99.99%) particles with a mean size of 0.6 μm and 50-63 μm 304L stainless-steel particles, composite particles with a spherical shape and an average diameter, after sieving, of 65 μm were obtained. They were composed of an alumina shell about 2 ± 4 μm thick with a 316L stainless-steel core.

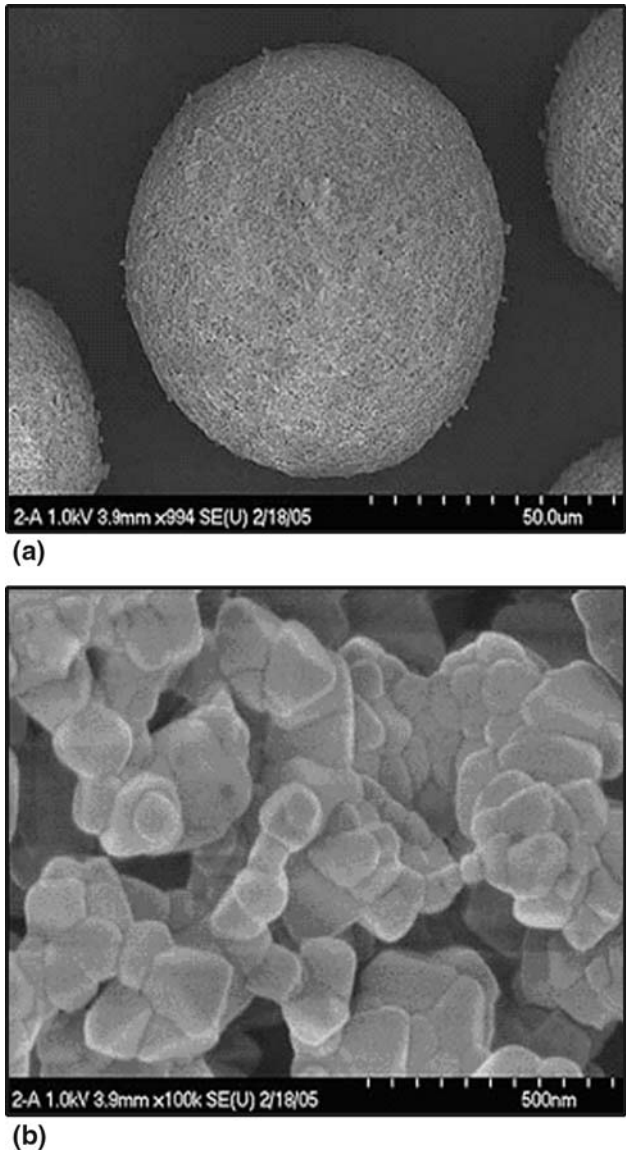

Fig. 3 (a) YSZ feedstock particle formed by the agglomeration (spray-drying) of individual nanometer-sized particles. (b) Particle depicted in (a) observed at higher magnification showing individual nanometer-sized YSZ particles in the 30-130 nm range (Ref 52)

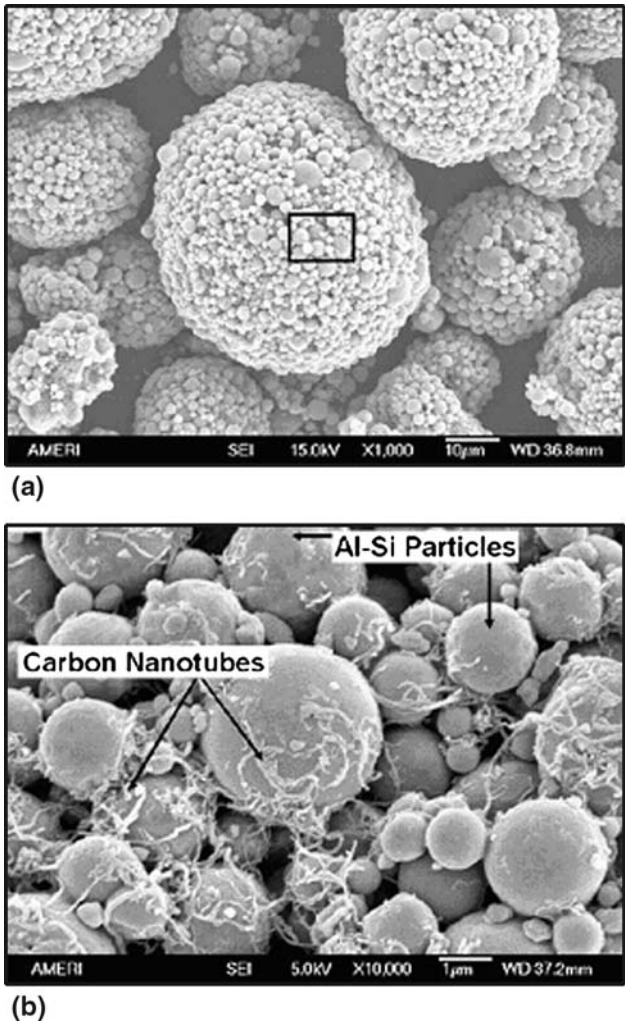

Fig. 4 (a) Spray-dried Al-Si agglomerate. (b) Magnified region within the rectangle in (a) showing CNTs within the agglomerate (Ref 53)

Clad composite powders enable the combination of high hardness and high toughness materials such as the ones forming cermet (ceramic-metal) composite particles (Ref 57). For example WC-Co (6 wt.%, instead of the conventional 17 wt.%) spray-dried particles are cobalt clad (11 wt.% of the whole particle) by CVD (chemical vapor deposition). The CVD coating technology utilizes fluidized beds to deposit coatings from inorganic metal precursors. The aim of the process is based on the fact that by decreasing the size of the reinforcement phase (which leads to the reduction in metal mean free path), the overall hardness of the cermet material increases with reducing grain size (for a given metal content). With WC-Co, since the ductile phase is distributed around the ceramic particles, forcing the metal mean free path (i.e., the effective metal grain size) to about 1/6th to 1/10th of the ceramic particle size provides, for adequate mean free path for the ductile binder phase, important improvements in toughness. In the clad particle, the removal of some of the ductile binding phase from the composite core, and its distribution at the meso-scale as a cladding on the core, allows two mean free paths to being generated in the same structure.

2.9 Sol-Gel

Sol-gel route can produce ceramic powders, especially oxides (alumina, chromia, stabilized zirconia, etc.), with a high surface area, which allows sintering to nearly full density at much lower temperatures than are normally required when the particles have been manufactured by other techniques (Ref 2, 33). It also allows, when considering particles with different components, such as

yttria-stabilized zirconia (YSZ), having them mixed at the nanometer level increasing the nontransformable tetragonal phase stability (Ref 22).

2.10 Particle Spheroidization

Using dense and spherical particles for spraying results in (i) much better flowability inducing more regular powder feed rate; (ii) dense particles with less heat propagation, especially when the particle thermal conductivity is low (Ref 58); (iii) less wear of pipes and feeding systems due to smoother particle surfaces and thus less coating contamination by impurities; (iv) a lower particle void content due to reactions with warm gases or vaporization, eliminating or at least reducing impurities (in a factor of 10-100 in the ppm range).

2.10.1 Conventional Particles (Micrometer-Sized Solid Particles). Spherical and dense particles are most of the time obtained by treating powders with thermal plasmas (Ref 59). Among the different possible routes, the most convenient one is RF discharge for the following reasons: (i) low plasma flow velocity (about 50 m s^{-1}) resulting in residence times almost one order of magnitude larger than in d.c. arcs; (ii) long residence times allowing using argon to reduce the heat transfer from the plasma thus limiting the heat propagation phenomenon; (iii) possibility to use almost any gas in the sheath gas, for example oxygen to keep the stoichiometry of SiO_2 particles. The set-up (Ref 60, 61) developed by Tekna for particle spheroidization, Fig. 5, comprises the plasma torch where particles are injected axially at the level of the mid-height of the coil, a water-cooled reservoir which length is adapted to permit particle solidification before reaching the container bottom (their velocity is roughly that of their free fall) and a cyclone followed by a filter collecting the smaller particles entrained by the gas flow.

Besides the heat and momentum transfers, described in details by Boulos et al. (Ref 62), two important points must be underlined: (i) radiative losses increase with the particle melting point and size, as illustrated in Fig. 6 (Ref 61) and (ii) loading effect since the increase in the powder flow rate cools down the plasma flow through the energy necessary to both melt and vaporize them (Ref 63), the latter being the more important for the smallest particles (Ref 63).

Thus, the maximum quantity of powder particles that can be spheroidized depends upon the torch power level, as illustrated in Table 1 (Ref 61). As in all industrial processes, the cost of spheroidization depends on the material to be treated, its size, the degree of spheroidization required and the quantity to be treated and it can vary in a factor of 10 (Ref 61). Figure 7 illustrates the shape of different particles before and after spheroidization. Figure 8 presents an industrial installation with a power level of 400 kW used by Teckna (Boucherville, QC, Canada) for particles spheroidization (Ref 63). However, it is very difficult to spheroidize particles prone to decompose such as hydroxyapatite (Ref 64).

2.10.2 Production of Spherical Particles from Suspensions. When chemical routes are implemented to process materials, crystallites are generally at the nanometer-scale. It is hence not simple to achieve dense and spherical powders from them, moreover without decomposing them. Bouyer et al. (Ref 65) have proposed the densification of hydroxyapatite by RF plasma (50 kW from Tekna, Boucherville, QC, Canada). The artificial HA is synthesized by wet-chemistry and the resulting aqueous precipitate (Fig. 9a) is concentrated by centrifugation and heated until reaching a percentage of solid in the suspension of about 40 wt.%. The suspension properties are then adjusted for decreasing its viscosity down to 0.4 Pa s. The suspension is fed via a peristaltic pump and is gas

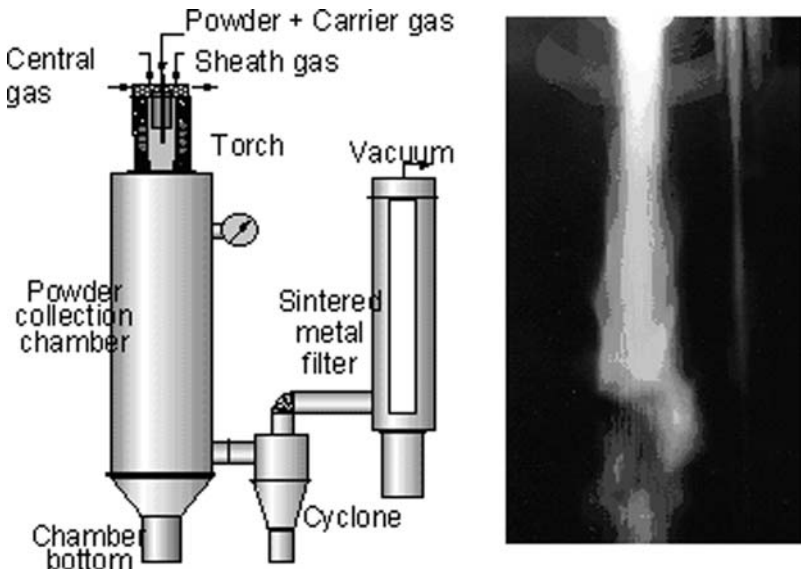

Fig. 5 Set-up developed by Teckna for powder spheroidization by RF plasma discharge with a picture of the jet and particles in-flight (Ref 60, 61)

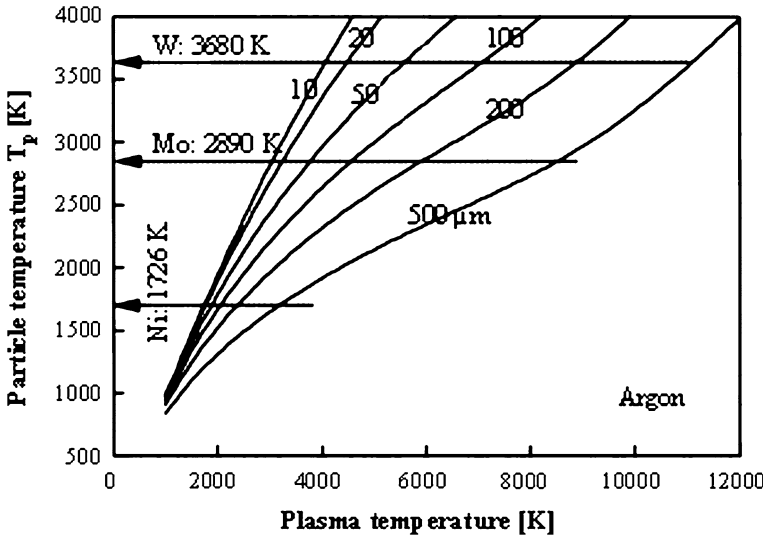

Fig. 6 Radiative losses from metal particles in an infinite plasma of pure argon (Ref 61)

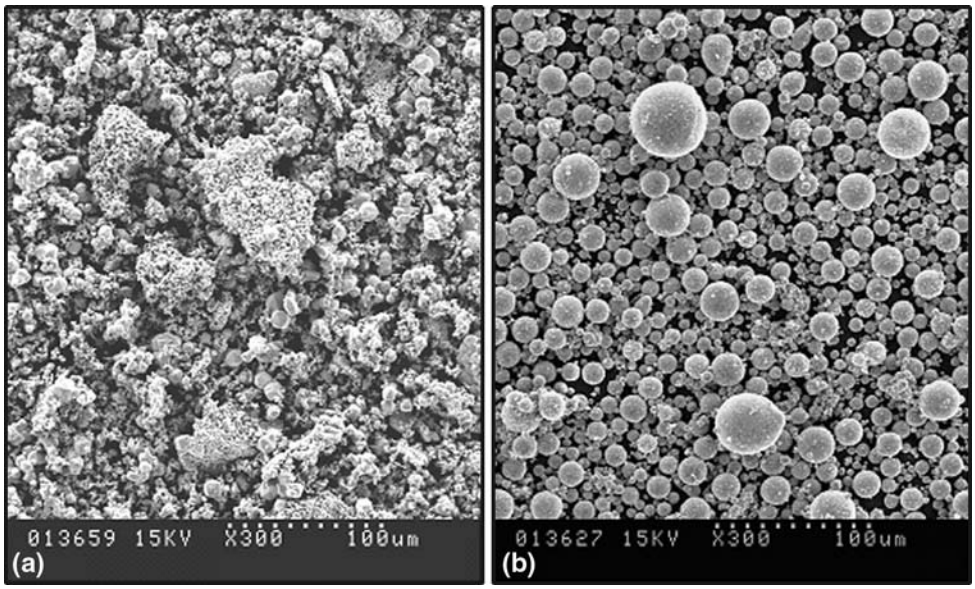

Fig. 7 Molybdenum particles (a) before spheroidization, (b) after spheroidization (Ref 61)

Table 1 Maximum powder flow rates which can be spheroidized (Ref 12)

Power, kW	65	125	400
Powder flow rate, kg h^{-1}	1-6	5-30	20-60

atomized to produce drops of 90 µm average size. The treatment of particles is presented schematically in Fig. 10. According to the low velocity of the plasma, the Weber number of particles is below 14 and they are not fragmented during their flight. The water is evaporated and the solid particles flash sintered and then melted, resulting in spherical particles with a 30 µm average size (Fig. 9b).

$LaMnO_3$ particles have been produced by RF plasma suspension spraying (Ref 66). However, they were partially decomposed in spite of the oxygen sheath gas. On the contrary $La_{0.8}Sr_{0.2}Mo_{3-\delta}$ particles for solid oxide fuel cells (SOFCs) cathode material have been successfully produced (Ref 67).

3. Coatings

3.1 Introduction

Thermal spray coatings result from stochastic processes. Except for cold spray, particles are accelerated and

then melted (totally or partially), before impacting onto the prepared substrate where they flatten and form flattened lamellae, called splats, from the layering of which results the coating (Ref 68). Particles melting occur in rather short times (a few milliseconds) and their solidification in even shorter times (a few microseconds) with strong temperature gradients and cooling rates in the 10^6-10^9 K s^{-1} range resulting sometimes in metastable or amorphous phases (Ref 69). Moreover, the spray pattern, the standoff distance (or spray distance), the control of the temperature time evolution (in the tenth of seconds response time) of the substrate before spraying (preheating), of the substrate and coating during spraying, of both when they cool down after spraying, allow tailoring the different residual stresses and their relaxation in the coating and substrate. Finally, the coating microstructure is very complex with many features such as voids, cracks (intra-lamellar failures), delamination (inter-lamellar failures), and interfaces of different length scales. Thus, coating properties do not only depend on the powder morphology, even if it is an important parameter.

Cold-sprayed particles must be accelerated to velocities higher than the so-called critical velocity, for a given diameter, to bond to the substrate and then the previously deposited layers (Ref 70). Coating properties are also linked to the peening effect of the impacting particles on the already deposited ones. Compared to thermal spraying, particle morphologies play a more important role when considering cold-gas spraying, according to the deformation properties of impacting particles (Ref 71). Cold-spray coatings present very low density of micrometer-sized features and low oxygen contents, and therefore exhibit bulk-like properties with respect to electrical or thermal conductivity (Ref 70).

3.2 Particles Injection

3.2.1 Micrometer-Sized Particles. Two types of injection are used, axial or radial, depending upon the spray torch design. In both types of injection particles are fed with a carrier gas through an injector. Consequently, they collide between themselves and the injector wall. It results that at the injector exit particle velocities, v_p, are about the same whatever are their size (Ref 72) and the average velocity depends upon the carrier gas flow rate and the injector internal diameter at exit. This means that, for a given carrier gas flow rate, the particle momentum, $m_p \times v_p$, varies as the cube of their diameter. For a size distribution between 22 and 44 μm, the cube of diameters ratio is 8, while for particles between 10 and 100 μm it becomes 1000! Thus the broader the size distribution, the more different the particle momentums at injector exit and so the larger the particle trajectories distribution and thus their velocity and temperature distributions at impact on the substrate. At last, beside its diameter, the particle mass also depends upon its specific mass, ρ_p, which depends itself upon the particle morphology, in particular its void content. For axial injection, the initial particle momentums condition the final velocities and temperatures imparted to them by the energetic gases, for

Fig. 8 Picture of an industrial set-up of 400 kW for powder spheroidization at Teckna (Ref 61)

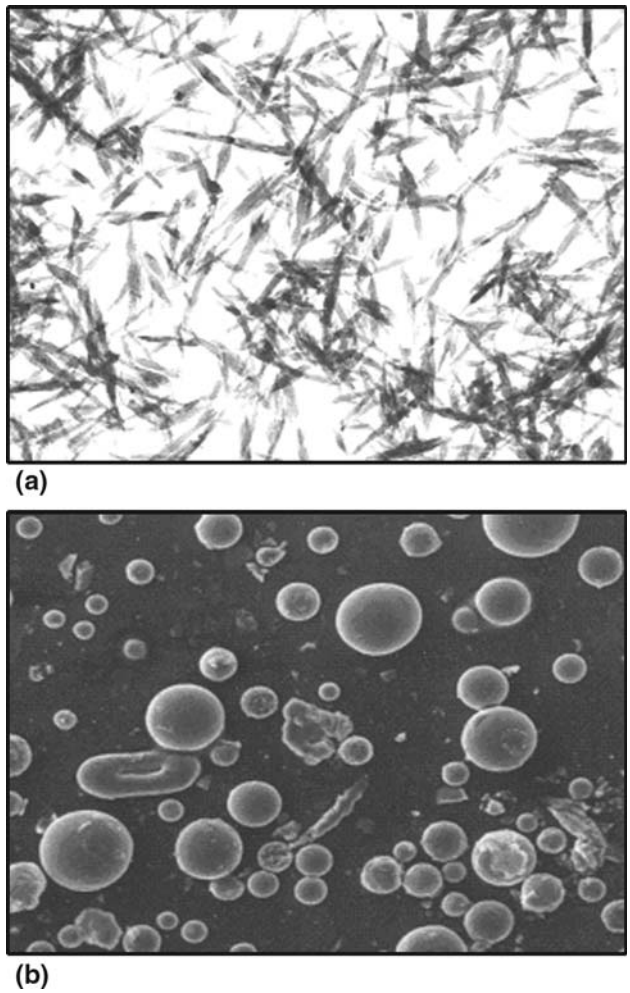

Fig. 9 (a) TEM picture of the as-synthesized HA nanocrystals. (b) SEM picture (top view of powders) of suspension RF plasma sprayed HA powders (Ref 61)

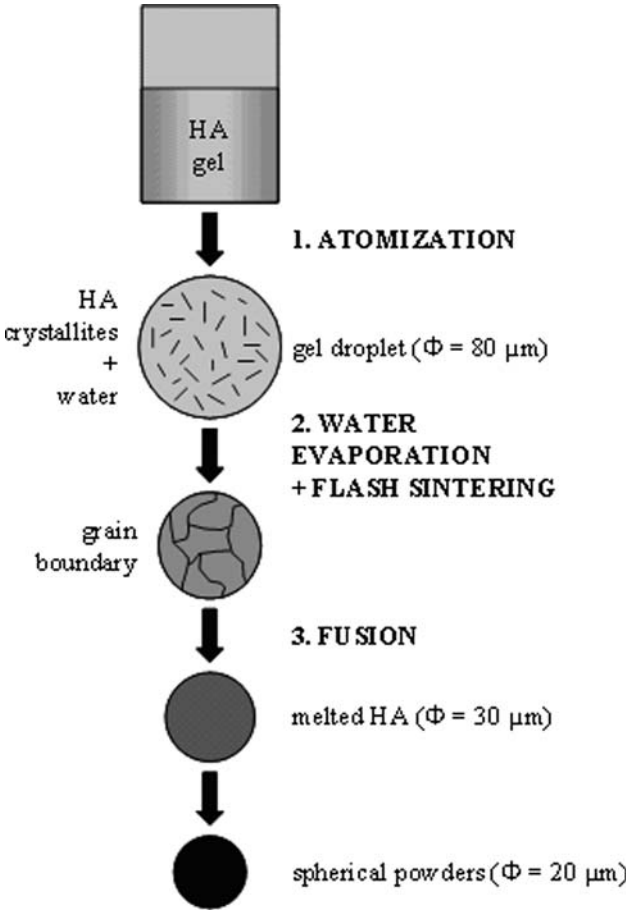

Fig. 10 Synthesis process of HA particles (Ref 65)

example, the calculations of Han et al. for cold-gas spraying (Ref 73). For radial injection, the optimum particle injection corresponds to an injection momentum that is about the same as that imparted to them by the energetic gas flows. It means that the carrier gas flow rate must be adjusted to any variation of the power spray parameters (Ref 72, 74). This is achieved by using different types of particle state sensors (Ref 75, 76). Of course the carrier gas flow rate must be increased when the particle size decreases, but below 5-10 µm particle average diameters, the energetic flow can be disrupted by the cold carrier gas at the injection point.

Another issue relies in the particle shape influence on its acceleration. For hot gases spraying, it is currently admitted that after a few millimeters trajectory, the particles are melted and thus spheroidized. In cold-gas spraying however, where particles are not heated or kept at temperatures below a few hundreds degrees, the particle shape plays a relevant role. For example, angular particles of both stainless-steel and bronze powders were traveling significantly faster (~80 m s^{-1}) than spherical particles (Ref 77). Gu and Kamnis obtained similar results for HVOF spraying with a high velocity torch (inducing few melting of particles) fed with liquid fuel and oxygen (Ref 78).

3.2.2 Sub-Micrometer or Nanometer-Sized Particles. The only way to inject dispersed sub-micrometer- or nanometer-sized particles is to use a liquid as carrier medium in which they are in suspension. Suspension spraying is actually mostly performed with plasma or HVOF processes. Spray conditions are somewhat more complex than those of conventional spraying. They depend on the suspension penetration within the hot gases jet, its fragmentation and resulting droplets penetration within the hot gases jet. Moreover, the strong cooling of the hot gases by liquid vaporization and the very low inertia of particles implies very short spray distances (from 30 to 60 mm, average values) corresponding to thermal fluxes imparted to the substrate by hot gas flow up to 25 MW m^{-2} (Ref 79).

3.3 Particle Reactions In-Flight

3.3.1 Involved Phenomena. Except in cold-gas spraying, for which particle surface temperature does not exceed a few hundreds of degrees, maximum value, particles react with their surrounding atmosphere, especially air where most spray processes take place. Those reactions are mostly controlled by diffusion or convection.

Diffusion tailors particle reactivity when the partial pressure of reactive gases in the flow surrounding the particle reaches a specific value, called critical pressure, the flux of reactive gases toward the surface of the melted particle exceeds the counter flux of feedstock vapor and a liquid or solid oxide, carbide or nitride layer, depending upon the nature of the reactive gases, forms at the surface of the droplet and vaporization ceased (Ref 80). According to Arrhenius law, the reaction kinetics increases drastically with temperature (about one order of magnitude for a temperature increase of 100-200 °C). Thus, for example, oxidation is rather high in plasma spraying, where particles are often over melted, and decreases in HVOF spraying, especially with high power torches (working with kerosene) where particle temperatures are rather low (close or below the melting point) and velocities over 500 m s^{-1}.

Convection tailors particle reactivity when velocity difference between a molten particle in-flight and the warmer surrounding gases can induce a convective motion within the particle. It occurs in plasma, HVOF, and wire arc spraying under certain conditions (Ref 81). This phenomenon can increase drastically the reaction rate (in a ratio up to 5) compared to pure diffusion.

It is also possible to use basic reactants in the solid phase either as agglomerated or clad particles (Ref 39, 82). Heating of the particle by warm gases triggers (it is the ''match'') the self-propagation high-temperature synthesis (SHS).

3.3.2 Diffusion-Controlled Reactions. As long as the particle is not melted, in the first millimeters of its trajectory convective movement within the particle induced by the warm gas flow is not possible. Farther downstream, the warm gas average velocity decreases and convection movements ceased. Thus, at the beginning and end of particle trajectory, chemical reactions are controlled by diffusion while in the middle of trajectory convective

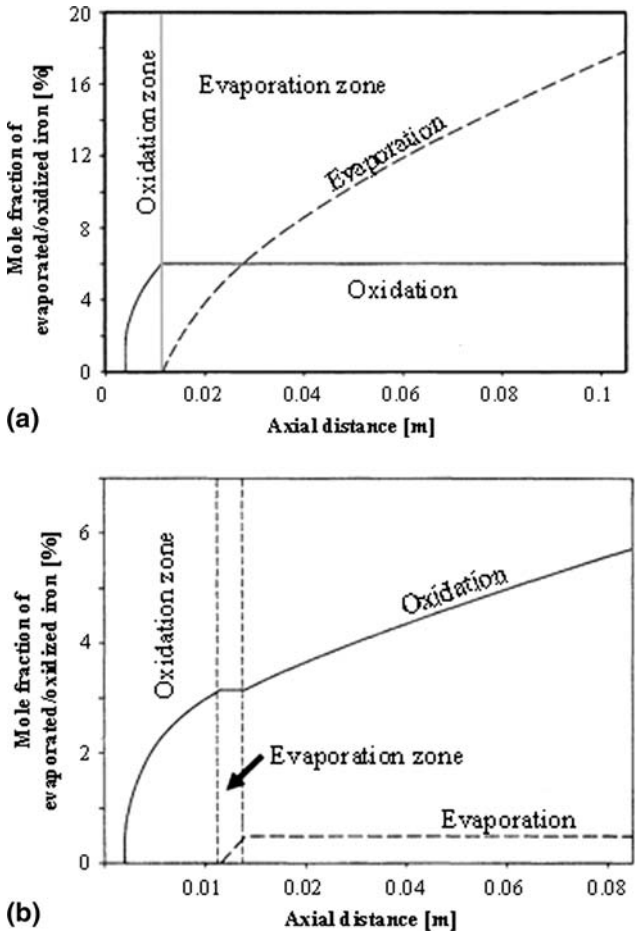

Fig. 11 Mole fraction of evaporated and oxidized iron along particle trajectory. (a) Initial particle size: 40 μm, injection velocity: 10 m s^{-1}. (b) 80 μm, injection velocity: 10 m s^{-1} (Ref 83)

reaction can occur in plasma, HVOF, and wire arc spraying. If convective conditions are not fulfilled (Ref 81), diffusion occurs all along the particle trajectory.

For pure diffusion two phenomena take place, evaporation with the oxidation of the vapor and oxidation of the particle. This is illustrated in Fig. 11 (Ref 83) for low carbon iron particles, produced by gas atomization, injected into an Ar-H_2 d.c. plasma jet (Ar-H_2 plasma jet, 600 A, 65 V, Ar-H_2 45-15 SLPM, anode nozzle internal diameter 7 mm). Figure 11 shows the mole fraction of evaporated and oxidized iron along the torch axial distance for two particle diameters, 40 and 80 μm, respectively, injected both at the same velocity of 10 m s^{-1}. This implies that if the trajectory of the 40 μm particle is optimum, the 80 μm particle will cross earlier the jet and thus will be less heated. This results in a much lower evaporation in the latter case with a strong oxidation while it is the opposite for the smaller particle diameter.

The compound formed at the particle surface depends upon the reactants present within the plasma (provided that they can diffuse to the particle surface through the boundary layer) and also very strongly upon the particle temperature. The diffusion phenomena occurring at the interfaces must be taken into account, diffusion of the reactant through the shell formed from reactions at the particle surface (in liquid or solid state) on the one hand and diffusion of gaseous reaction products formed (if any) through the shell and then through the boundary layer (see the shrinking core model described; Ref 84) on the other hand. The diffusion coefficients can be strongly modified by the expansion mismatch between the nonreacted particle core and the reacted shell formed around the core that can be easily broken if it is in the solid phase on a molten metal core. A few examples of oxidation can be found in Ref 85 and 86.

For cermets, such as WC-Co, the main phenomena that occur during thermal spray processes and which influence the coating performance are the oxidation and high-temperature decomposition of tungsten carbide (WC) giving rise to the formation of di-tungsten carbide (W_2C) as well as a high concentration of metallic tungsten (W) dissolved in the binder phase. These phenomena are promoted when the particle temperature increases over its melting temperature. For example when comparing the same WC-12 wt.% Co powder sprayed by high-velocity oxy-fuel (HVOF) and high-velocity air-fuel (HVAF), a substantial amount of W_2C was identified in the HVOF coatings, as well as a high concentration of tungsten in the binder phase (Ref 87). It indicates that oxidation and dissolution processes change the composition and microstructure from powder to coating during spraying. In contrast with HVAF spraying, where particles temperature is lower and velocity higher, composition and microstructure of coatings were unchanged from that of the powder. Additionally, the wear resistance of the HVAF coatings was superior to that of the HVOF coatings. It has also been shown that WC-17 wt.% Co coatings were not primarily influenced by variations in the spray parameters, but were more dependent on the powder composition, particle size range, and manufacturing route (Ref 88). Coatings manufactured with sintered and crushed powder delivered a more consistent and a lower wear rate than the agglomerated and densified powder type, but this effect was possibly related more to the WC grain size (respectively, 1 and 2.6 μm) than to the manufacturing route. De Villiers Lovelock (Ref 16) has presented a review of the work performed before 1998 on the phase changes that occur during spraying WC-12 wt.% Co and WC-17wt.% Co coatings, and differences obtained when using cast and crushed, sintered and crushed, and agglomerated and densified powder types. Similar works were performed on the influence of composition and microstructure of agglomerated and sintered (AS) WC-VC-Co powders, on coatings sprayed by HVOF (Ref 89). When HVOF spraying WC-Co (6 wt.%, instead of the conventional 17 wt.%) spray-dried particles cobalt clad (11 wt.%) (Ref 57), the wear resistance (using Tabor abrasive test to characterize fretting resistance) of the coating was close to that obtained with hard chromium.

Spraying metal particles in controlled atmosphere containing hydrocarbons or nitrogen produce many other species such as carbides or nitrides: TiC + Ti, SiC + Si, W + W_xC_y, Mo + MoC_2, NiCr/Ti + TiC + Cr_xC_y, FeCrAlY +

$Cr_xFe_y + Fe_xC_y$, $Mo + MoSi_2$, $Ti + TiB_2$, etc. (Ref 90-97). Of course the reaction must occur in solid or liquid phase and not in gas phase such as that producing AlN.

3.3.3 Convection Controlled Reactions in Fully Melted Particles. As already underlined, convective motion within the molten particle occurs only under certain conditions (Ref 81). The motion inside the particle can be represented by a Hill vortex that is an in-viscid axisymmetric vortex (Ref 98). For a low carbon 60 µm iron particle in a d.c. Ar-H_2 plasma jet, calculation was performed by using a commercial code, FIDAP7-62, dedicated to the materials processing field (Ref 98). Figure 12 shows the time resolved modeling of internal convection and oxide penetration by the spherical Hill vortex. The internal circulation in the droplet continuously sweeps fresh liquid to the particle surface to make it available for oxidation and entrains fragments of the outer oxide layer or of the dissolved oxygen at the particle surface inside the particle. With low carbon iron particles the oxide formed inside is liquid Fe_xO. Liquid iron and liquid Fe_xO are not miscible due to their difference in surface tension (1778 mJ m^2 for pure iron and 585 mJ m^2 for the wüstite; Ref 98). Thus upon cooling both phases separate and spherical Fe_xO nodules are formed within the particle as shown in Fig. 13. The re-circulating flow within the droplet results is an increase of the oxygen content compared to that estimated assuming a pure diffusion model (Ref 98). For example, under spraying conditions recalled in Fig. 12 caption, the captured FeO mass percentage is 15 wt.%, while diffusion calculations estimate the Fe_2O_3 and Fe_3O_4

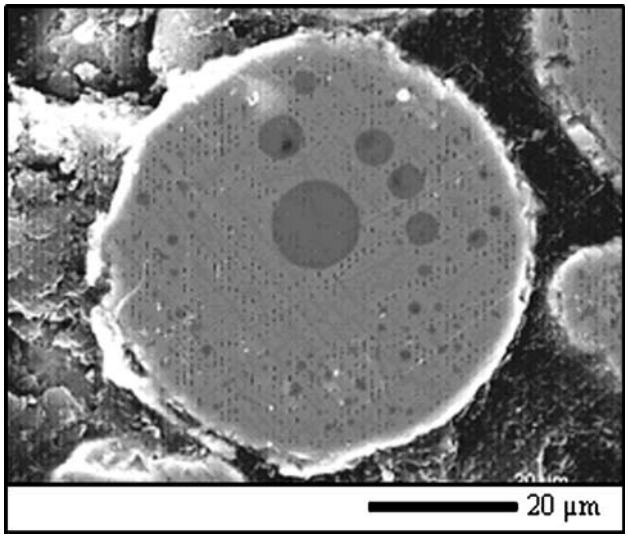

Fig. 13 Cross sections of a low carbon particle collected at $z = 100$ mm after its flight in a D.C. plasma jet: Ar 50 SLPM, H_2 10 SLPM, $I = 500$ A, nozzle i.d. 7 mm. SEM analysis at 30 keV. Scale 20 µm (Ref 98)

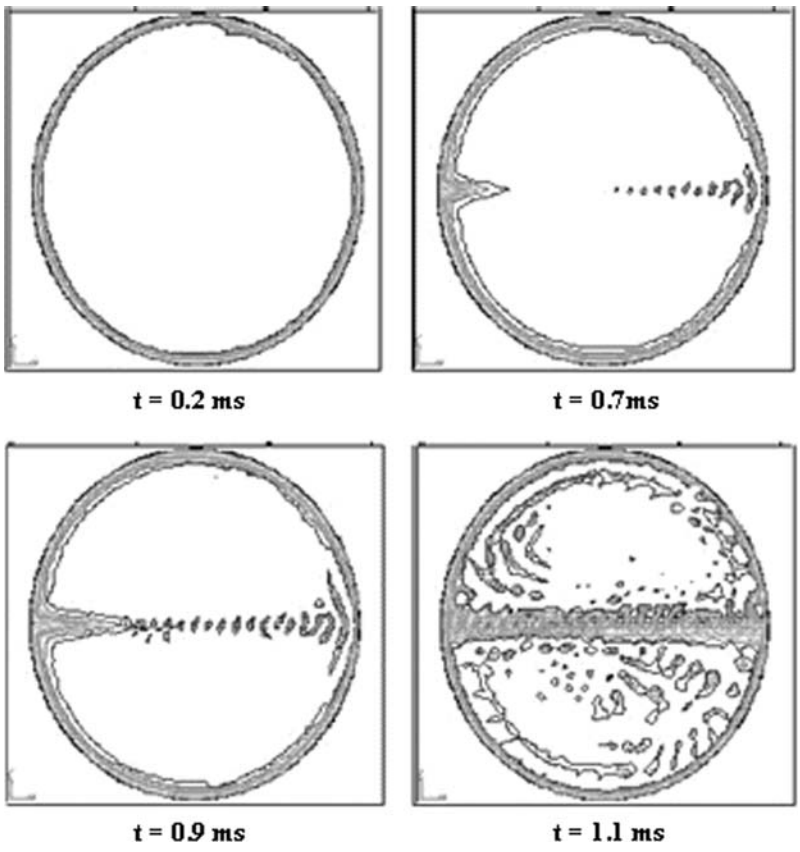

Fig. 12 Time-resolved modeling of internal convection and oxide penetration by a spherical vortex of Hill (Ref 98)

concentration to be less than 3 wt.%. The oxide shell formed at the surface of particles, with no inside convective movement, is made of Fe_2O_3 and Fe_3O_4. Such oxides are observed in the thin shell surrounding the particle (Fig. 13) formed at the end of the particle trajectory when the particle velocity is about the same as that of the surrounding plasma plume (no more convective effect). The corresponding coatings were harder (about 20% higher) than those obtained when spraying in argon atmosphere and their adhesion on stainless-steel slightly better, probably due to the better wettability of oxidized drops. The same effect was observed with stainless-steel particles plasma sprayed with Ar-H_2 plasma forming gas (Ref 86).

Similar results with convection have been observed when spraying Ti-6Al-4V (gas atomized) particles in a d.c. nitrogen plasma either under controlled atmosphere or in air. Inside the particles TiN and TiO were formed with, of course, much less TiO in controlled atmosphere (Ref 93).

3.3.4 Reactions Taking Place Between Condensed Phases (SHS). In this case, the basic reactants are in the solid phase either as agglomerated or cladded particles (Ref 82, 99-101). For the most common clad Ni-Al particle upon melting, Al reacts with the Ni creating intermetallics species such as Ni_3Al, NiAl, etc. through an exothermic reaction. The same holds for agglomerated particles of Ti and C for example (Ref 82). Plasma heating of the particle triggers the reaction that strongly depends upon the size of agglomerated particles and the possibility to heat the agglomerated particles without fragmenting the agglomerates by the produced gas expansion. As the speed of SHS is typically between 0.1 and 15 cm s^{-1}, the SHS reaction propagation is not necessarily completed during the flight of particles and it may proceed after their impact resulting in very dense and hard coatings (Ref 101).

Many coatings have been produced by this method; see for example the review of Borisova and Borisov (Ref 39):

- transition metal nonmetal refractory compounds with mixtures of Cr and SiC or B_4C, Ti and SiC or B_4C or Si_3N_4 producing coatings with silicides, carbides, borides which exhibit excellent resistance to wear (Ref 102-105);
- copper-TiB_2 coatings starting from agglomerated particles of Ti-bronze and boron, the TiB_2 particles in coatings increase considerably the hardness of copper matrix (Ref 104);
- TiB_2 or TiC particles in ferrous matrices to increase their hardness and wear resistance (Ref 105);
- Al and metal oxides to produce intermetallics with aluminum particles (Ref 106).

3.4 Coatings Manufactured from Conventional Micrometer-Sized Sprayed Particles

3.4.1 Conventional Coatings. The first case to be considered deals with thermally sprayed coatings manufactured with micrometer-sized ceramic particles. As already emphasized, the powder morphology has a great influence on coating properties, especially for ceramics and cermets (Ref 107). Most ceramic particles are either FC or agglomerated by spray drying and then sintered (resulting in spherical and sometimes hollow spheres [HOSP]). For example, Streibl et al. (Ref 108) have studied with different sensors the temperatures and velocities of YSZ particles sprayed with a 3 MB plasma torch (Sulzer-Metco, Wohlen, Switzerland) working with a plasma gas mixture of nitrogen and hydrogen. The particles used were commercial HOSP, FC and AS, all of them with about the same average diameter (d_{50} of the particle size distribution) and the carrier gas was optimized for each type of them. In-flight measurements have shown that the HOSP particles were indeed the easiest to melt compared to the others. This better heating is due to the lower mass of HOSP particles (the specific mass of such particles can be below 1000 kg m^{-3}) compared to that of other types of particles (AS and FC), the particle surface, the heat transfer coefficient from the warm gases being the same. Measurements of thermal conductivities κ_i (Ref 109) of corresponding coatings showed that, in the 200-1200 °C temperature range, $\kappa_{HSOP} < \kappa_{AS} < \kappa_{FC}$ pointing out the important role of inter-lamellar delaminations. HOSP particles result in thinner lamellae and consequently a larger fraction of inter-lamellar delaminations. Bertrand et al. (Ref 110) have compared also YSZ HOSP with an extremely low-specific mass (390 kg m^{-3} to be compared to 2000 kg m^{-3} for the commercial HOSP particles and to 2900 kg m^{-3} for FC particles). A decrease in 30% of as-sprayed apparent κ was obtained, as compared to a standard value, when spraying them (after spray conditions optimization). Wang and Shaw (Ref 11) have studied three Al_2O_3-TiO_2 powders with the same chemical composition, but different Al_2O_3-TiO_2 distribution patterns due to different manufacturing methods (spray-drying, FC, and plasma fused) on coating properties. The degree of mixing of the alumina and titania initial particles changes with the powder manufacturing method. It is particularly important for the particles degree of melting, the thermal conductivity of the resulting particles being increased with the better mixing of alumina and titania. It also affects the coating microstructure. TiO_2 lamellae and TiO_2-rich γ-Al_2O_3 regions can be eliminated if the sprayed powder is a mixture of both elements mixed at the submicrometer level.

The second case to be considered deals with thermally sprayed coatings manufactured with micrometer-sized composite particles: as problems linked to carbide-metal composites have been already discussed in Section 3.3, only one example of metal-oxide cermet will be detailed here. A typical mechanofused alumina-steel particle is presented in Fig. 14(a) (Ref 56, 111, 112). The starting 316L stainless-steel particles with an average diameter of 56 μm are coated with 2 ± 4 μm thick pure α-alumina (99.99%) particles of 0.6 μm average diameter. Upon spraying both materials are fully melted, and the lighter alumina at the steel core is entrained by the flow either before or behind the steel particle depending on its mass. It results in steel spheres with an alumina cap, as shown in Fig. 14(b). For particles below about 60 μm, the steel hits the substrate first and two lamellae are formed: a

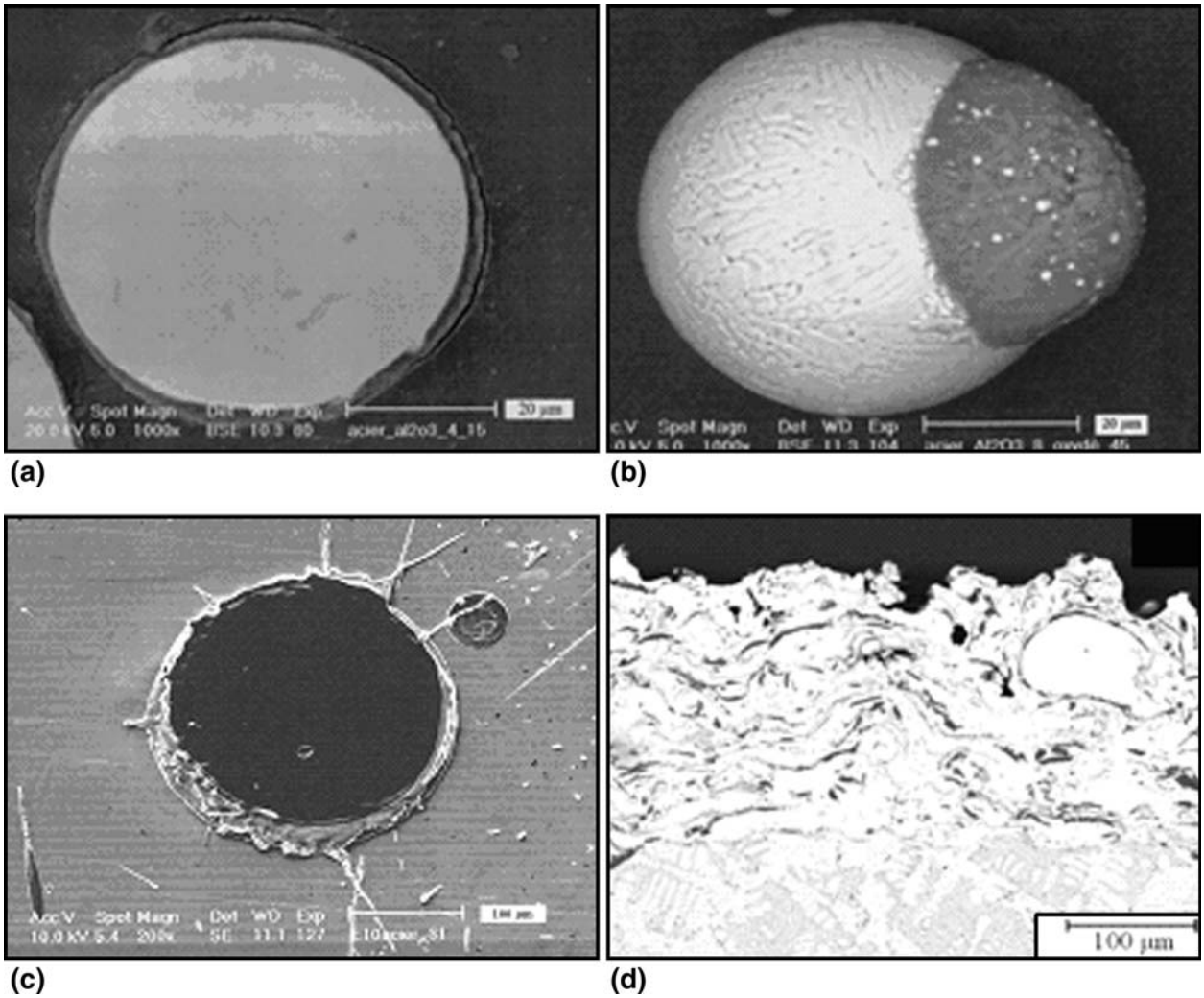

Fig. 14 Mechanofused alumina-stainless-steel coatings, (a) particle cross section, (b) particle collected after its flight into an Ar-H_2 plasma jet, (c) lamellae collected on a smooth substrate (alumina in black color and stainless-steel in gray color), (d) coating cross section with 6 wt.% alumina (Ref 112)

stainless-steel one on which lays an alumina one as shown in Fig. 14(c). Finally, the coating is made of layered steel and alumina lamellae as shown in Fig. 14(d). Compared to a pure stainless-steel substrate sprayed in the same conditions, the hardness of the alumina-stainless-steel coating is 620 ± 30 HV_5 against 660 ± 20 HV_5. To underline the effect of particles in-flight oxidation, the hardness of the bulk casted identical steel is only 450 ± 15 HV_5.

The third case to be considered deals with cold-gas sprayed coatings manufactured with micrometer-sized ceramic particles. The influence of various parameters (particle diameter, specific mass, material specific heat, etc.) on the critical velocity and deposition efficiency were studied systematically (Ref 113-121). The deposition efficiency increases with the particle temperature at impact for the same velocity (temperature increase implies Young's modulus reduction over values depending on materials). The critical velocity diminishes with increasing process gas temperature. It can be seen that increasing the particle temperature by 530 °C increases the Ni deposition efficiency by about 13% for the different velocities considered (Ref 122). Particle oxidation is also very important as shown by Kang et al. (Ref 123). The corresponding critical velocity for deposition of aluminum particles with different oxidation stages (varying the oxygen content from close to 0 to 0.04 wt.%) on aluminum substrates varied from 750 m s^{-1} to more than 850 m s^{-1}.

3.4.2 Totally or Partially Nanostructured Coatings. The first case considered is related to thermally sprayed coatings manufactured from micrometer-sized agglomerated nanometer-sized ceramic particles. Lima and Marple have recently published (Ref 50) a very complete overview on this topic. Without melting partially particles it is extremely difficult, if not impossible, to produce thermal spray coatings, particularly with ceramic materials. In order to overcome this challenge, it is necessary to carefully control the temperature of the particles in the thermal spray jet to keep part of them in a semi-molten state (Ref 58). As shown in Fig. 15 (Ref 50), the coating microstructure is formed by semi-molten

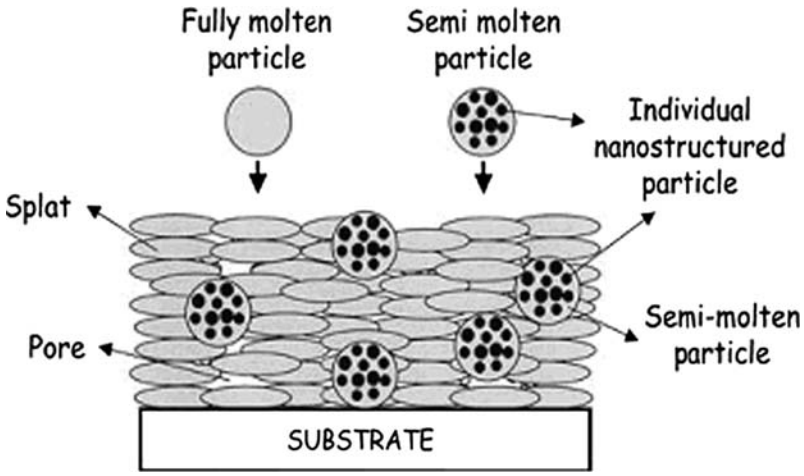

Fig. 15 Typical schematic (cross section) of the bimodal microstructure of thermal spray coatings formed by fully molten and semi-molten nanostructured agglomerated particles (Ref 50)

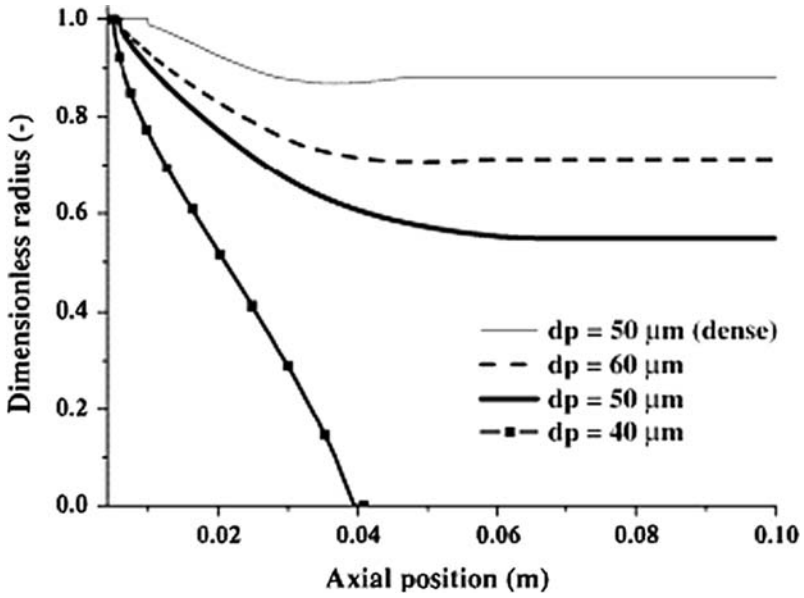

Fig. 16 Axial evolution of the melting front in agglomerated zirconia particles of different diameter (for comparison the evolution has been represented for a dense zirconia particle 50 μm in diameter). For the four cases, the particle trajectory was assumed to be the same (Ref 58)

feedstock particles that are spread throughout the coating microstructure and are surrounded by fully molten particles that act as a cement or binder. Some authors have described these two-scale coatings as exhibiting a ''bimodal'' microstructure.

For example calculations (Ref 58) have been made for dense (5680 kg m^{-3}) and porous (2840 kg m^{-3}) zirconia particles sprayed in a D.C. Ar-H_2 plasma jet. Figure 16 presents the axial evolution of the melting front within three agglomerated zirconia particles of different sizes. It allows evaluating the size of the nanostructured core, preserved at the end of the heat treatment of zirconia particles. The particle 40 μm in diameter is totally melted after 40 mm axial trajectory, when within particles of 50 and 60 μm keep nanostructured solid cores of 27 and 56 μm diameter are kept, corresponding to 54% and 71% of their initial diameter, respectively. Comparatively, dense zirconia particle, 50 μm in diameter, melts much more than the porous particle due to the better heat propagation.

The process optimization is facilitated by the use of diagnostic tools for monitoring the in-flight particle characteristics (Ref 75, 76). Spraying nanostructured powders with less control of temperatures may become possible if compensated by a significant high particle velocity (e.g., HVOF particle velocities) (Ref 52).

Figure 17 illustrates the coating two-scale (bimodal) microstructure obtained with plasma sprayed agglomerated nanometer-sized particles (Ref 50). Lighter-color and darker-color zones in the coating microstructure can be distinguished (Fig. 17a). In the latter, it is possible to recognize the morphology of the nanometer-sized YSZ feedstock (Fig. 2b). Lima and Marple (Ref 50) point out that by controlling the size, shape, and morphology of the bimodal distribution, it is possible to engineer coatings with very pronounced differences in microstructural characteristics and mechanical performances. A key parameter is the density of the nanometer-sized zones which can be dense or porous. The dense nanometer-sized zones (Fig. 18) (Ref 124) probably occur when there is significant infiltration of the molten part of a semi-molten particle into the small capillaries of its nonmolten core during thermal spraying (Ref 50). Porous nanometer-sized zones are obtained when using very porous nanostructure agglomerated particles. The control of particle melting is more difficult with plasma spraying (Ref 52) than with HVOF (Ref 52) in spite of the fact that spraying ceramic materials by HVOF is a challenge. This is due to the high melting point of ceramic materials and the low flame temperatures of HVOF torches (<3000 °C). Moreover, fine feedstock powders (5-25 μm average diameter) must be employed. Nevertheless, abrasion wear performance of HVOF-sprayed nanostructured titania or alumina-titania coatings are excellent. Compared to titania or alumina-titania conventional (i.e., micrometer-scale, one-scale structure) coatings, those made with nanostructured agglomerated particles, either plasma (Ref 52, 125-130) or HVOF (Ref 52, 131-133) sprayed, have better abrasion or sliding wear performance (Ref 50). Zirconia nanostructured plasma sprayed coatings have also been used against wear. The nanostructure coating reduced wear rate of the friction pair materials (Ref 134, 135). For more information on the advantages and drawbacks of these nanostructure coatings used for abradable, thermal barrier, biomedical coatings, see the review of Lima and Marple (Ref 50).

The second case considered is related to thermally sprayed coatings manufactured from cermet micrometer-sized particles made of agglomerated nanometer-sized particles. Even under HVOF spraying conditions of WC-Co particles with nanometer-sized WC, the extent of

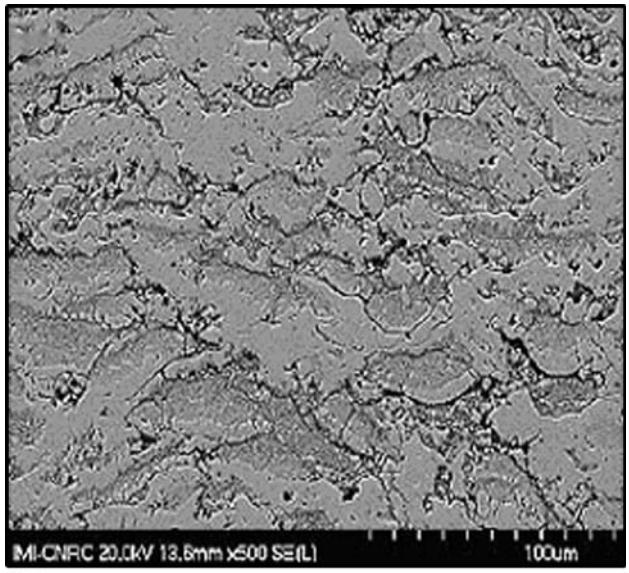

(a)

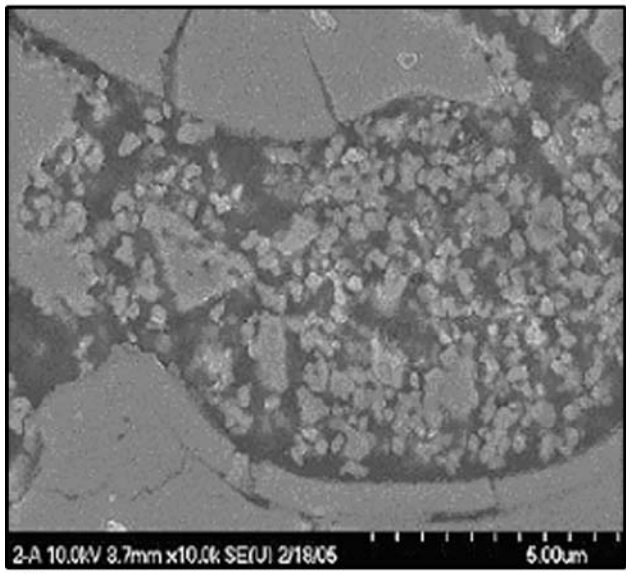

(b)

Fig. 17 (a) Microstructure of the nanostructured zirconia-yttria coating made from a nanostructure feedstock (Fig. 2) (Ref 59). (b) Darker-color regions containing the semi-molten feedstock particles (Ref 52)

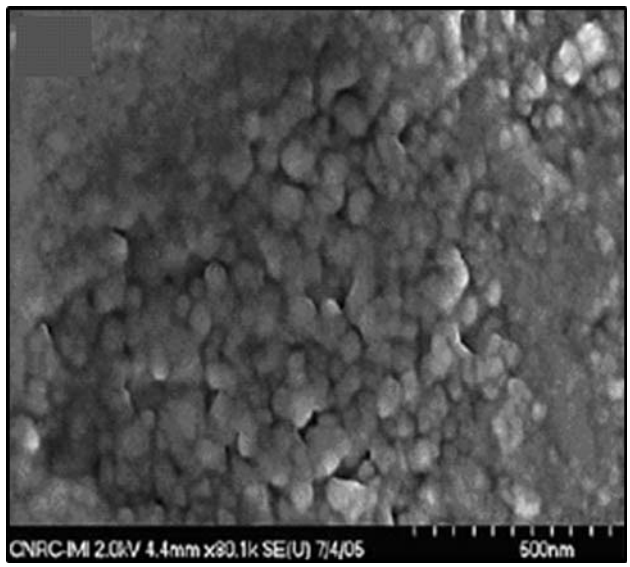

Fig. 18 Cross section at high magnification of a zone showing a semi-molten nanostructure of an HVOF-sprayed coating made from a nanostructured feedstock (124)

decarburization observed in is larger (because of particles higher specific surface) than that in the micro-sized coating material. However, many works have been devoted to this topic mainly by HVOF (Ref 136-138) and d.c. plasma spraying (Ref 139). With nanostructured WC-Co powders manufactured recently, the amount of the non-WC/Co phases was greatly reduced within coatings. A grain-growth inhibitor has a strong influence on the microstructure and other properties of the coatings. Preventing WC dissolution in the binder, not only maintains very small grains, but also maintains their original shape. However if it is effective in retarding decarburization, it decreases the cohesion between WC and binder.

Nanostructured Cr_3C_2-25(Ni20Cr) coatings are synthesized using mechanical milling and sprayed by HVOF or HVAF. Their decomposition seems to be less than that of WC-Co, better results being obtained with coatings sprayed by HVAF (Ref 140). Nanocrystalline coating exhibits 20% increase in hardness, 40% decrease in surface roughness, and comparable fracture toughness and elastic modulus with respect to conventional coating (Ref 141).

By HVOF spraying, Y_2O_3-reinforced milled FeAl (Ref 142), TiC-Ni-based composite (Ref 47), Al_2O_3 and Al_2O_3-Ni (Ref 143, 144) resulting in high quality coatings when optimizing spray parameters.

By plasma spraying, Al_2O_3 dispersed in a FeCu or FeCuAl matrix (Ref 145) appeared to offer a better wear resistance under sliding and abrasion tests than nanostructured Al_2O_3 coatings. Nanostructured YSZ/NiO anode provides larger triple phase boundaries for hydrogen oxidation reactions in SOFCs (Ref 146).

The third case considered is related to thermally sprayed coatings manufactured from alloy micrometer-sized particles made of nanometer-sized grains. Coatings are achieved with high power HVOF torch to keep as much as possible the nanocrystalline structure. Coatings present both nanocrystalline regions (grains of a few tens of nanometers) and submicron grain regions. The oxidation behavior of nanostructure NiCrAlY coatings, obtained from HVOF-sprayed cryomilled particles were investigated after heat treatments in air, at 1000 °C, for various times (Ref 147). Oxidation led to the formation of a continuous alumina layer, without the presence of other mixed oxides. Oxidation of nano-grain CoNiCrAlY coatings made from cryomilled powder was studied at, 1000 °C (Ref 148).

The fourth case considered is related to amorphous alloys. One has to distinguish here those containing additives such as phosphor, boron and silicon, that is to say compounds favoring amorphization from those made of complex compositions and nanoconsolidation.

Complex alloys containing phosphorus are known to present amorphous phases and can be produced by gas atomization. Alloy powders of Fe-10%Cr-8%P-2%C (10Cr), Fe-20%Cr-8%P-2%C(20Cr), and Fe-10%Cr-10%Mo-8%P-2%C(10Mo) compositions (in wt.%), obtained by atomization were sprayed by HVOF process under different conditions (Ref 149). Amorphous coatings with a small amount of crystalline phases were obtained from the 10Cr and 20Cr alloys and a 100% amorphous coating was formed from the 10Mo alloy.

Besides, and since the mid-eighties a few studies were devoted to the production and properties of air and vacuum plasma sprayed amorphous/nanocrystalline NiCrB and FeCrB based alloys (Ref 31). In-flight particle oxidation during atmospheric plasma spraying and HVOF spraying is however unavoidable. For example with NiTiZrSiSn, there is a preferential in-flight oxidation of Zr and Ti (Ref 150). As a matter of fact, preferential vaporization triggers the destabilization of the bulk metallic glass particle because amorphous phase stability and formability are largely affected by the chemical composition dependent critical cooling rate. With HVOF (H_2-O_2 mixture) (Ref 151) above a 0.20 O_2/H_2 ratio, severe oxidation is observed, inducing destabilization of the amorphous phase.

As explained previously, specialized iron-based compositions with a low critical cooling rate (10^4 K s^{-1}) for metallic glass formation have been developed. A primarily amorphous structure is formed in the as-sprayed coatings, independently of coating thickness. After a heat treatment above the crystallization temperature (568 °C which is less than half melting temperature), the structure of the coatings is devitrified into a multiphase nanocomposite microstructure with 75-125 nm grains containing a distribution of 20 nm secondary-phase grain-boundary precipitates. NanoSteel Company (Providence, RI, USA) was recently created to develop and market a range of high-performance patented super-hard steel materials that can be applied with a wide variety of processes: thermal spraying, welding (MIG and PTA), and laser cladding. They are mostly made of Fe-Cr-Mo-W-C-Mn-Si-B or of Cr-Mo-B-Si-W-Mn-C-Nb-Fe. Due to their high abrasion, erosion, and corrosion resistance, hardness and toughness, the main applications of such coatings are related to boiler tube refurbishments, hard chrome replacement, hard facing, pumps, etc. The SM2XS amorphous steel has been used successfully to replace hard chromium. Using HVOF good wear resistance was obtained in the three-body slurry abrasion tests (Ref 152). The SHS7574 powder was successively sprayed with D-gun and HVOF (Ref 152). A new iron-base cored wire, SHS7170, which readily forms nanocomposite coatings, was sprayed using the wire-arc process (Ref 153). The oxide content in the coatings is very low and is typically <1 vol%. Fe-based nano crystalline SHS7172CP1 (53-150 μm) solidifying wear-resistant materials have been clad on aluminum alloys using a cold arc PTA where the heat input into the base material and formation of spatter can be limited (Ref 154). The dilution is limited to approximately 5%, while the high conductivity of the base material is responsible for a high cooling rate, which induces nanocrystalline solidification.

The high cooling rate (10^6-10^9 K s^{-1}) during rapid solidification of molten powder in plasma spraying provides a high grain nucleation rate. However, the time for grain growth is not allowed, which results in extensive grain refinement. Viswanathan et al. (Ref 155) have presented a very complete review of nano-consolidated

coatings and only a few examples will be given in the following:

- Mixtures of hypereutectic Al alloy powder (50-100 μm) and nanometer-sized alumina powder (30-60 nm). Blending nanometer-sized alumina powders with micrometer-sized Al-Si powders eased the spraying of nanometer-sized powders as the micrometer-sized ones act as a carrier. Nanostructured aluminum oxide domains (20-50 nm size) were observed in the coating.
- Atmospheric plasma spraying of Mo powder resulted in formation of Mo/Mo oxide nanocomposite due to some oxidation of Mo. Fine particles of MoO_2 (5-10 nm) can be observed embedded randomly in the columnar grains of Mo.
- Freestanding bulk alumina nanocomposite with nanometer-sized Ni reinforcement were air plasma sprayed using Ni-coated Al_2O_3 powder as feedstock (30 nm thick nickel layer with 3-4 wt.% of Ni loading in the alumina matrix). The cross-sectional microstructure of the nanocomposite coating exhibited a 96-98% dense structure.

The fifth case considered is related to cold-gas sprayed nanometer-sized coatings manufactured with alloys or composites feedstock.

Nanocrystalline Al 5083 coatings were cold-gas sprayed with helium without preheating of the carrier gas (Ref 41) onto grit-blasted aluminum substrates. The critical velocity (over 700 m s^{-1}) was successfully achieved. The cold-sprayed coating showed negligible porosity and the interface with the substrate material was excellent. Cold-spray deposition of conventional and nanocrystalline (atomized and cryomilled) (Al-Cu-Mg-Fe-Ni-Sc) coatings was also successfully achieved (Ref 156). The conventional cold-sprayed coating showed negligible porosity and an excellent interface with the substrate material. This was not the case for the nanocrystalline coating, in which the porosity level was in the range of 5-10%. The microstructure of the feedstock powders was retained after the cold-spray process. The difference in porosity between the conventional and nanocrystalline coatings can be explained by the hardness and microstructure of the corresponding feedstock powder, which extent of deformation is much less, resulting in a less dense coating. The hardness of the nanocrystalline coating was similar to that of the feedstock powder, suggesting that no work hardening took place (Ref 156).

The metastable microstructure of the Fe(Al) feedstock, produced by ball milling and exhibiting a lamellar microstructure, was completely retained into the coating using cold spraying. The heat-treatment temperature has significant influence on the in situ evolution of the intermetallics compound. The FeAl intermetallics phase was formed during the heat treatment of the as-sprayed coatings at a temperature of 500 °C (Ref 157).

Nanocrystalline Al-Mg coatings were also produced using cold-gas spraying. The feedstock powder was characterized by a broad particle size distribution (10 μm to less than 100 μm) and was sprayed as-received, after the optimization of the spray parameters. ''Nanohardness'' values close to 3.6 GPa were observed in both the feedstock powder and coatings, suggesting the absence of cold-working hardening effects during the process (Ref 158). Moreover, this work demonstrates the ability of the cold-gas spray process to produce coatings on thin parts without noticeable substrate damage and with the same quality as coatings produced on thicker substrates.

The use of an amorphous Al-Co-Ce powder to produce nanostructured coatings with high degree of bonding to aluminum substrates alloys was demonstrated (Ref 159).

Nickel powder was mechanically milled in liquid nitrogen to achieve an average nanocrystalline grain size in the range of 20-30 nm. The powder was subsequently sprayed using cold-gas spraying (Ref 160). The nanocrystalline grain structure of the cryomilled feedstock powder was retained. Hardness values of 5.9 GPa were observed in the deposited nickel coatings and were comparable to electrodeposited nanocrystalline nickel coatings for the same range of grain sizes.

Nanostructured NiCrAlY starting powders were produced using a high-energy milling process, and subsequently a coating keeping feedstock nanostructure was deposited on IN738 substrate by cold-gas spraying (Ref 161). The shot-peened coating presented a rather good resistance to oxidation.

A commercial nanostructure WC-12Co powder with a nominal WC grain size of 50-500 nm (Inframat, Wellington, CT, USA) was sprayed on stainless-steel substrate (Ref 162). Critical velocities of about 915 m s^{-1} were measured for the present feedstock powder. The microhardness value of the as-sprayed coating was about 1800 $HV_{0.3N}$. It can be considered that a WC-Co powder with WC loosely bonded by the binder is suitable for cold-gas spraying to permit the pseudo-deformation through compaction of particles. The high velocity impact of WC-Co particles, induced the refinement of WC particles possibly through fracture of large WC particles.

Agglomerates of particles of aluminum-silicon eutectic alloy, in which multiwalled CNT were dispersed by spray drying (see spray-drying section) were mixed (Turbula-type mixer) with 99.7% pure Al powder (26 ± 13 μm) to generate powders for cold-gas spraying which contained an overall CNT content of 0.5 wt.% and 1 wt.%, respectively. Cold-sprayed coatings were successfully achieved onto aluminum alloy AA6061 substrate (Ref 53). CNTs were successfully retained and located both between the splat interfaces and also embedded in the matrix. However, CNTs were shortened in length due to fracture that occurs due to impact and shearing between Al and Si eutectic particles and the aluminum matrix. Values of the elastic modulus (obtained by nanoindentation) of coatings ranged between 40 GPa and 120 GPa. The lower values correspond to the porous regions of the coatings while the higher ones correspond to the Si rich regions. Locally some regions had elastic modulus as high as 229 GPa for Al-0.5 wt.% CNT and 191 GPa for Al-1wt.% CNT coating. It was attributed to the reinforcement effect of CNTs and the locally high level of CNTs in the region measured.

3.5 Coatings from Nanometer-Sized Sprayed Particles: Suspension Spraying

To produce finely structured ceramic or cermet (WC-Co) coatings of sub-micrometer-sized or nanometer-sized particles a suspension of these particles is thermally sprayed (Ref 79, 163-166). Spray conditions are somewhat more complex than those of conventional spraying because the suspension penetration within the hot gases jet, its fragmentation and resulting droplets penetration within the hot gases jet, the cooling of the hot gases and the very low inertia of sub-micrometer-sized or nanometer-sized particles, both implying very short spray distances (between 30 and 50 mm against 100-120 mm in conventional spraying), see the review of Fauchais et al. (Ref 79).

As in conventional spraying, the selection of the particles of the suspension is also a key issue. They should not agglomerate and have a rather narrow size distribution, moreover it is not yet clear what is the optimum particle size: in the tenths of micrometers or in the hundreds of micrometers. To illustrate the importance of the particle agglomeration are presented results obtained with two powders processed with highly fluctuating (''restrike'' mode) plasma jets were conducted: the first setting considered an Ar-H_2 ($\Delta V/V_m = 1.4$) plasma flow (Ar: 45 SLPM, H_2: 15 SLPM, I: 500 A, V: 65 V, h: 17.9 MJ kg^{-1}) and the second one a ternary Ar-H_2-He ($\Delta V/V_m = 0.7$) plasma flow (Ar: 40 SLPM, H_2: 10 SLPM, He: 50 SLPM, I: 500 A, h: 22.3 MJ kg^{-1}). The first considered powder was a TZ-8Y from Tosoh (Tokyo, Japan) of particle size distribution ranging from 30 to 80 nm (supplier data). The particles have the tendency to agglomerate or aggregate, modifying the apparent particle size distribution (Fig. 18a) that ranges from 50 nm to 3 μm (laser particle size analysis). The lamella average diameter distribution displayed also in Fig. 19 evolves from 0.3 to 2 μm.

Considering particle flattening ratio between 1.5 and 2.5 (Ref 164), this signifies that all particles smaller than 0.2 μm, average value, have either not been treated (melted) and have rebounded upon impact on the substrate or have been vaporized. However, spheres with characteristic sizes ranging from 0.1 to 0.7 μm (average size of 0.3 μm) were collected onto the substrate. Those spheres very likely result from the re-condensation of vaporized small particles. The coating architecture displayed in Fig. 19(b) exhibits a high level of voids mostly defined by columnar structures developing through the layer thickness, each column presenting 10 to 20 μm characteristic sizes. In the porous zones of 1 μm characteristic dimension, many small spherical particles of 0.2 to 0.3 μm characteristic sizes can be detected. Once again, such a typical structure is very likely linked to the vaporization of particles of 0.2 to 0.3 μm, average sizes, within the plasma warm core and to untreated particles traveling in the jet fringes and being poorly treated (this poor treatment being itself emphasized by the plasma jet fluctuations). Moreover, since no lamella of size larger than 2 μm is detected within the structure, this signifies that large agglomerates and aggregates have ''exploded'' with the flow upon heating.

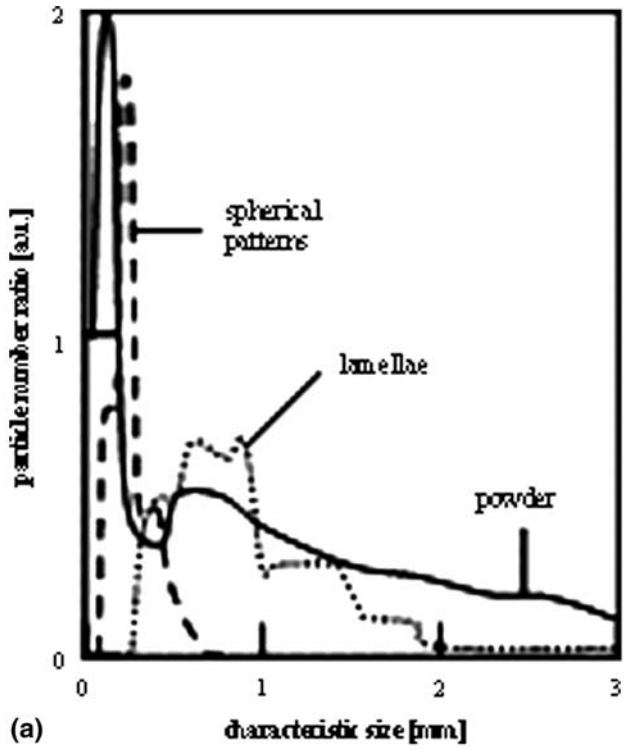

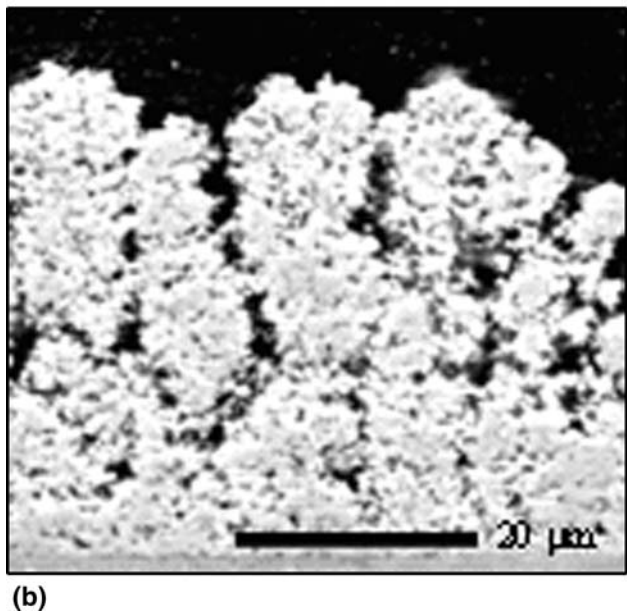

Fig. 19 (a) Particle, lamellae and spherical patterns size distribution. (b) Resulting coating architecture (TZ-8Y powder with broad particle size distribution due to the formation of aggregates)

The second considered powder is the same TZ-8Y that has been previously separated by sedimentation into de-ionized water, that is to say from which the smallest fraction of the particle size distribution has been discarded from the biggest one made of agglomerates and aggregates. The resulting particle size distribution is depicted in

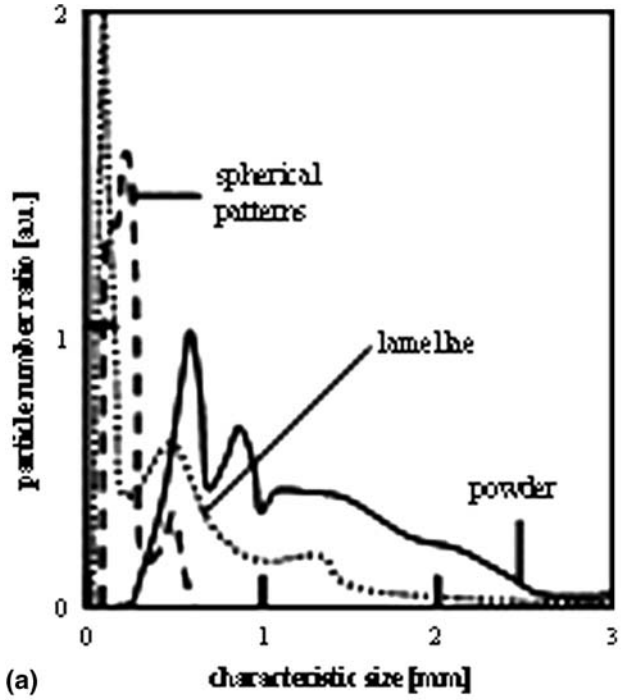

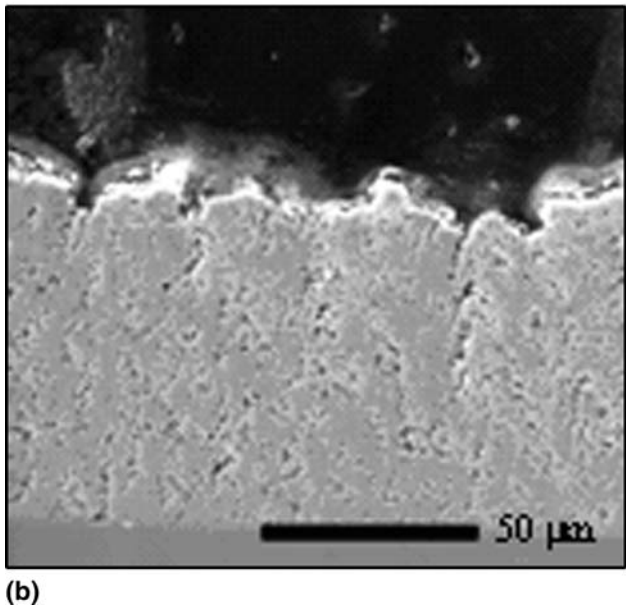

Fig. 20 (a) Particle, lamellae, and spherical patterns size distribution. (b) Resulting coating architecture (TZ-8Y powder with narrow particle size distribution resulting from sedimentation)

Fig. 20(a). Most of the particles exhibit average diameters ranging from 0.1 to 1 µm. Resulting lamellae, collected under the same conditions, have equivalent average diameter ranging from 0.3 to 2 µm. Here again, spherical particles of average diameters ranging from 0.1 to 0.5 µm are also collected. The structure of the coating manufactured with this narrower particle size distribution is displayed in Fig. 19(b): it is rather dense compared to the

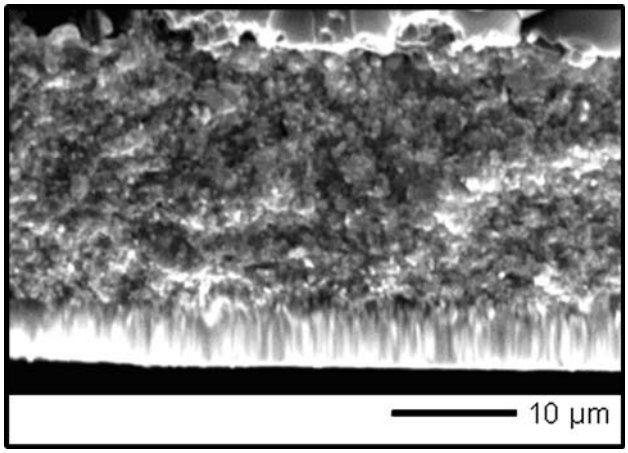

Fig. 21 Zirconia suspension plasma sprayed (Ar-H_2) onto a stainless-steel substrate and detached from its substrate prior fracture

previous considered one. Such an architecture results thank to lower plasma fluctuations and a narrower feedstock particle size distribution.

For YSZ coatings, the coating structure is quite different from that of conventional coatings made of layered lamellae. The four or five first micrometers close to the substrate presents a columnar structure, resulting from layered lamellae on the side of the stainless-steel substrate, followed by a granular structure (Fig. 21). The lamellar layer corresponds very likely to a good heat transfer through the stainless-steel substrate. However, once YSZ thickness has reached about these 5 µm, heat transfer is drastically reduced. According to the plasma heat flux (about 21 MW m^{-2}) imparted by the plasma flow under considered operating conditions, the new impacting fully molten particles are kept in a molten state during a time sufficiently long to recover a shape close to spherical due to the surface tension force.

Typical applications are described in the reviews of Fauchais et al. (Ref 79) and Gadow et al. (Ref 166).

4. Conclusion

Adapted powder to the spray process is one of the keys to good coatings. However, as in pastry a good flour is fundamental, the quality of the cake is strongly linked to the knowledge and experience of the cooker, it is the same with spraying. The powder characteristics (size distribution, shape, morphology, and specific mass) must be chosen according to the spray process used and spray parameters. For example when spraying WC-Co cermets, choosing atmospheric plasma spraying is not well adapted, the over-melting promoting WC dissolution in liquid Co and WC decomposition. However if the aim is to produce coatings with a rather low friction coefficient against an adapted material, carbon dissolved within the cobalt matrix is interesting. The best choice to achieve cermets with WC particles homogeneously distributed within the

cobalt matrix is then using HVAF guns or high power HVOF guns, where particles are close to the melting point but with very high velocities (>500 m s^{-1}). The WC particle size is also an important issue; the smaller they are the easier they are prone to decompose. Thus, a compromise must be found or a grain-growth inhibitor, preventing WC dissolution in the binder, must be used, but the binder loosely bonds the WC particles. Among the recent developments in powders production cryomilling appears to be an important issue giving the possibility to obtain nanometer-sized ceramic particles and producing alloyed micrometer-sized particles with nano-sized grains. The manufacturing of complex new bulk amorphous alloys with a multicomponent chemistry and high GFA have been developed, especially in Fe-base systems with atomization and various rapid solidification techniques. They allow producing amorphous coatings by almost all thermal processes, coatings presenting nanostructures after reheating with very high hardness (not far from those of WC-Co cermets coatings). The recent industrial development of particles spheroidization by RF plasmas allows producing dense and spherical particles, mainly of refractory materials, for thermal spraying and powder metallurgy. At last the huge quantity of works devoted to the production of manometer-structured coatings must be underlined. All spray techniques are involved. Most developments are devoted to micro-sized agglomerated nano-sized particles or cryomilled particles and also to new suspension spraying process where nanometer-sized particles are injected with a liquid carrier. Of course the spray process has to be adapted. For example for cold spray, particles with a good deformation capacity, large particle size distribution, where big particles have a peening effect, etc. Cold-sprayed particles, in which multiwalled CNT are dispersed, seem to open interesting ways to coating reinforcement. For example, the YSZ nanostructure coatings obtained by suspension plasma or HVOF spraying are very promising for SOFC's electrolyte and thermal barrier coatings. To summarize new powder manufacturing techniques have showed-up recently, especially to spray nanostructure coatings. However between coating and powder the choice of the spray process and spray parameters is as important as the powder choice.

References

1. *Handbook of Powder Technology, Particle Breakage*, A. D. Salman, M. Ghadiri, and M.J. Hounslow, Ed., Elsevier B.V., Lausanne, Switzerland, 12, 2007, p 1-1227
2. *Handbook of Thermal Spray Technology*, J.R. Davis, Ed., ASM International, Materials Park, OH, USA, 2004
3. Anonymous, *Thermal Spraying, Practice, Theory and Application*, American Welding Society, Miami, FL, USA, 1985
4. L. Pawlowski, *The Science and Engineering of Thermal Spray Coatings*, Wiley and Sons, New York, NY, USA, 1995
5. E.J. Kubel, Powders Dictate Thermal Spray Coating Properties, *Adv. Mater. Processes.*, 1990, **12**, p 24-32
6. B. Kolman, J. Forman, J. Dubsky, and P. Chraska, Homogeneity Studies of Powders and Plasma Sprayed Deposits, *Mikrochim. Acta*, 1994, **114-115**, p 335-342
7. J. Wigren, J.F. de Vries, and D. Greving, Effects of Powder Morphology, Microstructure and Residual Stresses on Thermal Barrier Coating Thermal Shock Performance, *Thermal Spray: Practical Solutions for Engineering Problems*, C.C. Berndt, Ed., ASM International, Materials Park, OH, USA, 1996, p 855-861
8. A. Denoirjean, A. Vardelle, A. Grimaud, P. Fauchais, E. Lugsheider, I. Rass, H.L. Heijen, P. Chandler, R. McIntyre, and T. Cosak, Comparison of the Properties of Plasma Sprayed Stabilized Zirconia Coatings for Different Powder Morphologies, *Thermal Spray: International Advances in Coating Technology*, C.C. Berndt, Ed., ASM International, Materials Park, OH, USA, 1992, p 975-982
9. M.E. Vinayo, F. Kassabji, J. Guyonnet, and P. Fauchais, Plasma Sprayed WC-Co Coatings Influence of the Spray Conditions, *J. Vac. Sci.Technol.*, 1985, **3**(6), p 2483-2489
10. P. Diez and R.W. Smith, The Influence of Powder Agglomeration Methods on Plasma Sprayed Yttria Coatings, *J. Therm. Spray Technol.*, 1993, **2**(2), p 165-172
11. M. Wang and L.L. Shaw, Effects of the Powder Manufacturing Method on Microstructure and Wear Performance of Plasma Sprayed Alumina-Titania Coatings, *Surf. Coat. Technol.*, 2007, **202**, p 34-44
12. J. Beczkowiak and J. G. Schwier, Tailoring Carbides and Oxides for HVOF, *Thermal Spray: Coatings Properties, Processes and Applications*, C.C. Berndt and T.F. Bernecki, Ed., ASM International, Materials Park, OH, USA, 1991, p 121-126
13. P. Vuoristo, T. Mantyla, L.M. Berger, and M. Nebelung, Sprayability and Properties of TiC-Ni Based Powders in the Detonation Gun and HVOF Processes, *Thermal Spray: A United Forum for Scientific and Technological Advances*, C.C. Berndt, Ed., ASM International, Materials Park, OH, USA, 1997, p 909-915
14. W.J. Jarosinski, M.F. Gruninger, and C.H. Londry, Characterization of Tungsten Carbide Cobalt Powders and HVOF Coatings, *Thermal Spray Coatings: Research, Design and Applications*, C.C. Berndt and T.F. Bernecki, Ed., ASM International, Materials Park, OH, USA, 1993, p 153-157
15. M.C. Kim, S.B. Kim, and J.W. Hong, Effect of Powder Types on Mechanical Properties of D-Gun Coatings, *Thermal Spray: A United Forum for Scientific and Technological Advances*, C.C. Berndt, Ed., ASM International, Materials Park, OH, USA, 1997, p 791-795
16. H.L. de Villiers Lovelock, Powder/Processing-Structure Relationships in WC-Co Thermal Spray Coatings: A Review of the Published Literature, *J. Therm. Spray Technol.*, 1998, **7**(3), p 357-373
17. P. Suresh Babu, D.S. Rao, G.V.N. Rao, and G. Sundararajan, Effect of Feedstock Size and Its Distribution on the Properties of Detonation Sprayed Coatings, *J. Therm. Spray Technol.*, 2007, **16**(2), p 281-290
18. M. Yandouzi, L. Ajdelsztajn, and B. Jodoin, WC-Based Composite Coatings Prepared by the Pulsed Gas Dynamic Spraying Process: Effect of the Feedstock Powders, *Surf. Coat. Technol.*, 2008, **202**, p 3866-3877
19. I.E. Anderson, D.J. Sordelet, M.F. Besser, and R.L. Terpstra, Effects of Powder Morphology on Pneumatic Feeding and Plasma Spray Deposition, *Thermal Spray: Meeting the Challenges of the 21st Century*, C. Coddet, Ed., ASM International, Materials Park, OH, USA, 1998, p 911-916
20. X. Fan, F. Gitzhofer, and M.I. Boulos, Statistical Design of Experiments for the Spheroidization of Powdered Alumina by Induction Plasma Processing, *J. Therm. Spray Technol.*, 1998, **7**(2), p 247-253
21. M. Vardelle, A. Vardelle, and P. Fauchais, Spray Parameters and Particle Behavior Relationships During Plasma Spraying, *J. Therm. Spray Technol.*, 1993, **2**(1), p 79-92
22. P. Boch, P. Fauchais, D. Lombard, B. Rogeaux, and M. Vardelle, Plasma Sprayed Zirconia Coatings, *Ad. Ceram.*, 1985, **12**, p 488-503
23. D.J. Sordelet, M.F. Besser, M.J. Kramer, S. DePalo, and S. Sampath, Thermal Spray Quasicrystalline Coatings. Part 1: Relationships Among Processing Phase Structure and Splat Morphology, *Thermal Spray: Meeting the Challenges of the 21st Century*, C. Coddet, Ed., ASM International, Materials Park, OH, USA, 1998, p 467-472

24. D. Sordelet and M. Besser, Effect of Starting Powder Particle Size and Composition on Chemistry and Structure of Al-Cu-Fe Quasicrystalline Plasma Sprayed Coatings, in *Thermal Spray: Practical Solutions for Engineering Problems*, C.C. Berndt, Ed., ASM International, Materials Park, OH, USA, 1996, p 419-428
25. Y. Wang, R.S. Lima, C. Moreau, E. Garcia, J. Guimaraes, P. Miranzo, and M.I. Osendi, Mullite Coatings Produced by APS and SPS: Effect of Powder Morphology and Spray Processing on the Microstructure, Crystallinity and Mechanical Properties, *Thermal Spray 2009: Expanding thermal spray performance to new markets and applications*, B.R. Marple, M.M. Hyland, Y.-C. Lau, C.-J. Li, R.S. Lima, and G. Montavon, Ed., ASM International, Materials Park, OH, USA, 2009, p 97-102
26. P. Pei, J. Kelly, S. Malghan, and S. Dapkunas, Analysis of Zirconia Powder for Thermal Spray, *Thermal Spray: Practical Solutions for Engineering Problems*, C.C. Berndt, Ed., ASM International, Materials Park, OH, USA, 1996, p 263-73
27. J.J. Dunkley, Atomization, *Powder Metal Technologies and Applications*, ASM Handbook, ASM International, Materials Park, OH, USA, 1998, p 35-52
28. A.V. Sergueeva, D.J. Branagan, and A.K. Mukherjee, Microstructure/Properties Relationship in Fe-Based Nanomaterials, *Mater. Sci. Eng. A*, 2008, **493**, p 237-240
29. D.J. Branagan, W.D. Swank, D.C. Haggard, and J.R. Fincke, Wear-Resistant Amorphous and Nanocomposite Steel Coatings, *Met. Mater. Trans. A*, 2001, **32A**, p 2615-2621
30. D.J. Branagan, M.C. Marshall, B.E. Meacham, L.F. Aprigliano, R. Bayles, E.J. Lemieux, T. Newbauer, F.J. Martin, J.C. Farmer, J.J. Haslam, and S.D. Day, Wear and Corrosion Resistant Amorphous/Nanostructured Steel Coatings for Replacement of Electrolytic Hard Chromium, *Building on 100 Years of Success: Proceedings of the 2006 International Thermal Spray Conference*, B.R. Marple, M.M. Hyland, Y.C. Lau, R.S. Lima, and J. Voyer, Ed., ASM International, Materials Park, OH, USA, 2006, e-proceedings
31. A.H. Dent, A.J. Horlock, D.G. McCartney, and S.J. Harris, The Corrosion Behavior and Microstructure of High-Velocity Oxy-Fuel Sprayed Nickel-Base Amorphous/Nano-Crystalline Coatings, *J. Therm. Spray Technol.*, 1999, **8**(3), p 399-404
32. H.M. Lee, C.Y. Huang, and C.J. Wang, Forming and Sintering Behaviors of Commercial α-Al_2O_3 Powders with Different Particle Size Distribution and Agglomeration, *J. Mater. Proc. Technol.*, 2009, **209**, p 714-722
33. Powders, Fibers, Platelets, and Composites, *Ceramic Materials, Chemistry and Materials Science Collection*, Springer, New York, NY, USA, 2007
34. C. Han, H. Choi, C. Lee, H. Kim, and S. Hwang, Evaluation of Solid Lubricant Coatings for Low Friction and Wear Resistance Using the Atmospheric Plasma Spray, *Mater. Sci. Forum*, 2004, **449**, p 777-780
35. X.-F. Zhang, X.-L. Zhang, A.-H. Wang, and Z.-W. Huang, Microstructure and Properties of HVOF Sprayed Ni-Based Submicron WS_2/CaF_2 Self-Lubricating Composite Coating, *Trans. Nonferrous Met. Soc. China*, 2009, **19**, p 85-92
36. C. Tekmen, I. Ozdemir, G. Fritsche, and Y. Tsunekawa, Structural Evolution of Mechanically Alloyed Al-12Si/TiB_2/h-BN Composite Powder Coating by Atmospheric Plasma Spraying, *Surf. Coat. Technol.*, 2009, **203**, p 2046-2051
37. M.A. Camerucci and A.L. Cavalieri, Process Parameters in Attrition Milling of Cordierite Powders, *J Mater. Synth. Proc.*, 1998, **6**(2), p 115-121
38. E.J. Lavernia, B.Q. Han, and J.M. Schoenung, Cryomilled Nanostructured Materials: Processing and Properties, *Mater. Sci. Eng. A*, 2008, **493**, p 207-214
39. A.L. Borisova and Yu.S. Borisov, Self-Propagating High-Temperature Synthesis for the Deposition of Thermal-Sprayed Coatings, *Powder Met. Met. Ceram*, 2008, **47**(1-2), p 80-94
40. C. Suryanarayana, Mechanical Alloying and Milling, *Prog. Mater. Sci.*, 2001, **46**, p 1-184
41. L. Ajdelsztajn, B. Jodoin, G.E. Kim, and J.M. Schoenung, Cold Spray Deposition of Nano-Crystalline Aluminum Alloys, *Metal. Mater. Trans. A*, 2005, **36A**, p 657-666
42. J.A. Picasa, A. Forna, L. Ajdelsztajnb, and J. Schoenung, Nano-Crystalline NiCrAlY Powder Synthesis by Mechanical Cryomilling, *Powder Technol.*, 2004, **148**, p 20-23
43. J. He and J.M. Schoenung, Nanostructured Coatings: A Review, *Mater. Sci. Eng. A*, 2002, **336**, p 274-319
44. K.H. Chung, J. He, D.H. Shin, and J.M. Schoenung, Mechanisms of Microstructure Evolution During Cryomilling in the Presence of Hard Particles, *Mater. Sci. Eng. A*, 2003, **356**, p 23-31
45. N. Eigen, T. Klassen, E. Aust, R. Bormann, and F. Gärtner, Production of Nano-Crystalline Cermet Thermal Spray Powders for Wear Resistant Coatings by High-Energy Milling, *Mater. Sci. Eng. A*, 2003, **356**, p 114-121
46. J. Oberste Berghaus, J.-G. Legoux, C. Moreau, F. Tarasi, and T. Chraska, Mechanical and Thermal Transport Properties of Suspension Thermal-Sprayed Alumina-Zirconia Composite Coatings, *J. Therm. Spray Technol.*, 2008, **17**(1), p 91-104
47. N. Eigen, F. Gärtner, T. Klassen, E. Aust, R. Bormann, and H. Kreye, Microstructures and Properties of Nanostructured Thermal Sprayed Coatings Using High-Energy Milled Cermet Powders, *Surf. Coat. Technol.*, 2005, **195**, p 344-357
48. D.E. Walton and C.J. Mumford, Spray Dried Products-Characterization of Particle Morphology, *Trans. Inst. Chem. Eng.*, 1999, **77**, p 21-38
49. G. Bertrand, P. Roy, C. Filiatre, and C. Coddet, Spray-Dried Ceramic Powders: A Quantitative Correlation Between Slurry Characteristics and Shapes of the Granules, *Chem. Eng. Sci.*, 2005, **60**, p 95-102
50. R.S. Lima and B.R. Marple, Thermal Spray Coatings Engineered From Nanostructured Ceramic Agglomerated Powders for Structural, Thermal Barrier and Biomedical Applications: A Review, *J. Therm. Spray Technol.*, 2007, **16**(1), p 40-63
51. R.S. Lima and B.R. Marple, Superior Performance of High-Velocity Oxy-Fuel-Sprayed Nanostructured TiO_2 in Comparison to Air Plasma-Sprayed Conventional Al_2O_3-13TiO_2, *J. Therm. Spray Technol.*, 2005, **14**(3), p 397-404
52. R.S. Lima, B.R. Marple, A. Dadouche, W. Dmochowski, and B. Liko, Nanostructured Abradable Coatings for High Temperature Applications, *Building on 100 Years of Success: Proceedings of the International Thermal Spray Conference 2006*, B.R. Marple, M.M. Hyland, Y.-C. Lau, R.S. Lima, and J. Voyer, Ed., ASM International, Materials Park, OH, USA, 2006, e-proceedings
53. S.R. Baksh, V. Singh, K. Balani, D.G. McCartney, S. Seal, and A. Agarwal, Carbon Nanotube Reinforced Aluminum Composite Coating Via Cold Spraying, *Surf. Coat. Technol.*, 2008, **202**, p 5162-5169
54. E. Lugscheider, M. Loch, and H. Eschnauer, Coated powders—The Status Today, *2nd Plasma-Technik Symposium*, P. Huber and H. Echnauer, Ed., Plasma Technik, Wholen, Ch. 2, 1991, p 339-351
55. H. Ito, M. Umakoshi, R. Nakamura, T. Yokoyama, K. Urayama, and M. Kato, Characterization of Ni-Al Composite Powders Formed by Mechanofusion, *Thermal Spray Coatings: Properties, Processes and Applications*, T.F. Bernecki, Ed., ASM International, Materials Park, OH, USA, 1991, p 405-411
56. H. Ageorges and P. Fauchais, Plasma Spraying of Stainless-Steel Particles Coated with an Alumina Shell, *Thin Sol. Films*, 2000, **370**, p 213-222
57. A.J. Sherman and P.G. Engleman, Metal Clad Cermet Powders: Processing and Properties, *Thermal Spray 2009: Expanding Thermal Spray Performance to New Markets and Applications*, Vol. 8, B.R. Marple, M.M. Hyland, Y.-C. Lau, C.-J. Li, R.S. Lima, and G. Montavon, Ed., ASM International, Materials Park, OH, USA, 2009, p 36-840
58. F. Ben-Ettouil, O. Mazhorova, B. Pateyron, H. Ageorges, M. El-Ganaoui, and P. Fauchais, Predicting Dynamic and Thermal Histories of Agglomerated Particles Injected Within a d.c. Plasma Jet, *Surf. Coat. Technol.*, 2008, **202**, p 4491-4495
59. B. Dzur, Plasma Puts Heat Into Spherical Powder Production, *Met. Powder Rep.*, 2008, **2**(63), p 12-15
60. http://www.tekna.com

61. M. Boulos, M. Ducos, and P. Fauchais, Plasma Technology and Its Potential for Powder Treatment, *Matériaux 2006*, 13-17 November 2006, Dijon, France, SF2M, Paris, France, 2006 (in French)
62. M. Boulos, P. Fauchais, A. Vardelle, and E. Pfender, Injection of Hot Particles in a Plasma Flame, *Plasma Spraying Theory and Applications*, R. Suryanarayanun, Ed., World Scientific, Singapore, 1993, p 3-61
63. N.M. Dignard and M.I. Boulos, Ceramic and Metallic Powder Spheroidization Using Induction Plasma Technology, *Thermal Spray: A United Forum for Scientific and Technological Advances*, C.C. Berndt, Ed., ASM International, Materials Park, OH, USA, 1997, p 1-7
64. J.L. Xu, K.A. Khor, and R. Kumar, Spheroidization of Bioceramic Powders in a Radio Frequency Plasma, *Thermal Spray 2007: Global Coating Solutions*, B.R. Marple, M.M. Hyland, Y.-C. Lau, C.-J. Li, R.S. Lima, and G. Montavon, Ed., ASM International, Materials Park, OH, USA, 2007, p 890-893
65. E. Bouyer, F. Gitzhofer, and M. Boulos, Suspension Plasma Spraying for Hydroxyapatite Powder Preparation by RF Plasma, *IEEE Trans. Plasma Sci.*, 1997, **25**(5), p 1066-1072
66. G. Schiller, M. Müller, and F. Gitzhofer, Preparation of Perovskite Powders and Coatings by Radio Frequency Suspension Plasma Spraying, *J. Therm. Spray Technol.*, 1999, **8**(3), p 389-392
67. D. Bouchard, L. Sun, F. Gitzhofer, and G.M. Brisard, Synthesis and Characterization of $La_{0.8}Sr_{0.2}MO_{3-\delta}$ (M = Mn, Fe, or Co) Cathode Materials by Induction Plasma Technology, *J. Therm. Spray Technol.*, 2006, **15**(1), p 37-45
68. P. Fauchais, Understanding Plasma Spraying: An Invited Review, *J. Phys. D Appl. Phys.*, 2004, **37**, p 2232-2246
69. P. Fauchais, M. Fukumoto, A. Vardelle, and M. Vardelle, Knowledge Concerning Splat Formation: An Invited Review, *J. Therm. Spray Technol.*, 2004, **13**(3), p 337-360
70. F. Gärtner, T. Stoltenhoff, T. Schmidt, and H. Kreye, The Cold Spray Process and Its Potential for Industrial Applications, *J. Therm. Spray Technol.*, 2006, **15**(2), p 223-232
71. T. Schmidt, F. Gärtner, H. Assadi, and H. Kreye, Development of a Generalized Parameter Window for Cold Spray Deposition, *Acta Mater.*, 2006, **54**, p 729-742
72. M. Vardelle, A. Vardelle, P. Fauchais, K.-I. Li, B. Dussoubs, and N.J. Themelis, Controlling Particle Injection in Plasma Spraying, *J. Therm. Spray Technol.*, 2001, **10**(2), p 267-284
73. T. Han, Z. Zhao, B.A. Gillispie, and J.R. Smith, A Fundamental Study of the Kinetic Spray Process, *Thermal Spray Solutions—Advances in Technology and Application*, DVS, Düsseldorf, Germany, 2004, e-proceedings
74. V. Srinivasan, M. Friis, A. Vaidya, T. Streibl, and S. Sampath, Particle Injection in Direct Current Air Plasma Spray: Salient Observations and Optimization Strategies, *Plasma Chem. Plasma Proc.*, 2007, **27**(5), p 609-623
75. V. Srinivasan, A. Vaidya, T. Streibl, M. Friis, and S. Sampath, On the Reproducibility of Air Plasma Spray Process and Control of Particle State, *J. Therm. Spray Technol.*, 2006, **15**(4), p 739-743
76. P. Fauchais, J.-F. Coudert, and M. Vardelle, Diagnostics of Plasma Spray Process and Derived On-Line Control, *High Temp. Mater. Proc.*, 2002, **6**(2), p 247-265
77. H. Fukanama, N. Ohno, B. Sun, and R. Huang, The Influence of Particle Morphology on In-Flight Particle Velocity in Cold Spray, *Building on 100 Years of Success: Proceedings of the International Thermal Spray Conference 2006*, B.R. Marple, M.M. Hyland, Y.-C. Lau, R.S. Lima, and J. Voyer, Ed., ASM International, Materials Park, OH, USA, 2006, e-proceedings
78. S. Gu and S. Kamnis, Numerical Modeling of In-flight Particle Dynamics of Non-Spherical Powder, *Surf. Coat. Technol.*, 2009, **203**, p 3485-3490
79. P. Fauchais, R. Etchart-Salas, V. Rat, J.-F. Coudert, N. Caron, and K. Wittmann-Ténèze, Parameters Controlling Liquid Plasma Spraying: Solutions, Sols or Suspensions, *J. Therm. Spray Technol.*, 2008, **17**(1), p 31-59
80. D.G.C. Robertson and A.E. Jenkins, The Reaction of Liquid Iron and Its Alloys in Pure Oxygen, *Heterogeneous Kinetics at Elevated Temperatures*, G.R. Belton and W.L. Workel, Ed., Plenum Press, New York, NY, USA, 1970, p 369-385
81. R.A. Neiser, M.F. Smith, and R.C. Dykhuisen, Oxidation in Wire HVOF-Sprayed Steel, *J. Therm. Spray Technol.*, 1998, **7**(4), p 537-545
82. S. Dallaire, Thermal Spraying of Reactive Materials to Form Wear-Resistant Composite Coatings, *J. Therm. Spray Technol.*, 1992, **1**(1), p 41-47
83. M. Vardelle, A. Vardelle, K.-I. Li, P. Fauchais, and N.J. Themelis, Coating Generation: Vaporization of Particles in Plasma Spraying and Splat Formation, *Pure Appl. Chem.*, 1996, **68**(5), p 1093-1099
84. J. Amouroux, A. Gicquel, S. Cavadias, D. Morvan, and F. Arefi, Progress in the Applications of Plasma Surface Modifications and Correlations with the Chemical Properties of the Plasma Phase, *Pure Appl. Chem.*, 1985, **57**(9), p 1207-1222
85. G. Espie, A. Denoirjean, P. Fauchais, J.-C. Labbe, J. Dudsky, O. Scheeweiss, and K. Volenik, In-Flight Oxidation of Iron Particles Sprayed Using Gas and Water Stabilized Plasma Torches, *Surf. Coat. Technol.*, 2005, **195**, p 17-28
86. A.A. Syed, A. Denoirjean, P. Denoirjean, J.-C. Labbe, and P. Fauchais, In-Flight Oxidation of Stainless Steel in Plasma Spraying, *J. Therm. Spray Technol.*, 2005, **14**(1), p 177-177
87. L. Jacobs, M.M. Hyland, and M. De Bonte, Comparative Study of WC-Cermet Coatings Sprayed Via the HVOF and the HVAF Process, *J. Therm. Spray Technol.*, 1998, **7**(2), p 213-218
88. H.L. de Villiers Lovelock, P.W. Richter, J.M. Benson, and P.M. Young, Parameter Study of HP/HVOF Deposited WC-Co Coatings, *J. Therm. Spray Technol.*, 1998, **7**(1), p 97-107
89. S. Luyckx and C.N. Machio, Characterization of WC-VC-Co Thermal Spray Powders and Coatings, *Int. J. Refrac. Met. Hard Mater.*, 2007, **25**, p 11-15
90. R.W. Smith and Z.Z. Matasin, Reactive Plasma Spraying of Wear-Resistant Coatings, *J. Therm. Spray Technol.*, 1992, **1**(1), p 57-63
91. T. Eckardt, W. Malleaer, and D. Stove, Reactive Plasma Spraying of Silicon in Controlled Nitrogen Atmosphere, *Thermal Spray: Industrial Applications*, C.C. Berndt and S. Sampath, Ed., ASM International, Materials Park, OH, USA, 1994, p 515-520
92. P. Fauchais, A. Vardelle, and A. Denoirjean, Reactive Thermal Plasmas: Ultrafine Particle Synthesis and Coating Deposition, *Surf. Coat. Technol.*, 1997, **979**, p 66-78
93. A. Denoirjean, P. Lefort, and P. Fauchais, Nitridition Process and Mechanism of Ti-6Al-4V Particles by Plasma Spraying, *Phys. Chem. Phys.*, 2003, **5**, p 5133-5138
94. D. Zou, D. Yan, L. Xiao, and Y. Dong, Characterization of Nanostructured TiN Coatings Fabricated by Reactive Plasma Spraying, *Surf. Coat. Technol.*, 2008, **202**, p 1928-1934
95. A. Kobayashi, Formation of TiN Coatings by Gas Tunnel Type Plasma Reactive Spraying, *Surf. Coat. Technol.*, 2000, **132**, p 152-157
96. M. Inagaki, Y. Yokogawa, and T. Kameyama, Bond Strength Improvement of Hydroxyapatite Titanium Composite Coating by Partial Nitriding During R.F.-Thermal Plasma Spraying, *Surf. Coat. Technol.*, 2003, **173**, p 1-8
97. M. Yamada, Y. Kouzaki, T. Yasui, and M. Fukumoto, Fabrication of Iron Nitride Coatings by Reactive R.F. Plasma Spraying, *Surf. Coat. Technol.*, 2006, **201**, p 1745-1751
98. G. Espié, P. Fauchais, B. Hannoyer, J.-C. Labbe, and A. Vardelle, Effect of Metal Particles Oxidation During the APS on the Wettability, Heat and Mass Transfer Under Plasma Condition, P. Fauchais, J. Van der Mullen, and J. Heberlein, Ed., *Ann. NY Acad. Sci.*, 1999, **891**, p 143-151
99. Y. Borisov and A. Borisova, Application of Self-Propagating High-Temperature Synthesis in Thermal Spraying Technology, *Thermal Spray: Research, Design and Applications*, T.F. Bernicki, Ed., ASM International, Materials Park, OH, USA, 1992, p 139-144
100. S.C. Deevi, V.K. Sikka, C.J. Swindeman, and R.D. Seals, Reactive Spraying of Nickel-Aluminide Coatings, *J. Therm. Spray Technol.*, 1997, **6**(3), p 335-344
101. B. Haller, J.-P. Bonnet, P. Fauchais, A. Grimaud, and J.-C. Labbe, TiC Based Coatings Prepared by Combining SHS and

Plasma Spraying, *Thermal Spray Connects: Explore its Surfacing Potential!*, E. Lugscheider, Ed., DVS-Verlag GmbH, Düsseldorf, Germany, 2005, e-proceedings
102. S. Dallaire, Influence of Temperature on the Bonding Mechanism of Plasma-Sprayed Coatings, *Thin Sol. Films*, 1982, **95**, p 237-241
103. Yu. Borisov, A. Borisova, and L.K. Shvedova, Transition Metal-Non Metallic Refractory Compound Composite Powders for Thermal Spraying, *Advances in Thermal Spraying*, Pergamon Press, Ottawa, Canada, 1986, p 323-329
104. J.G. Legoux and S. Dallaire, Copper-TiB_2 Coatings by Plasma Spraying Reactive Micropellets, *Thermal Spray: Research, Design and Applications*, C.C. Berndt and T.F. Bernecki, Ed., ASM International, Materials Park, OH, USA, 1993, p 429-432
105. S. Dallaire and G. Cliche, The Influence of Composition and Process Parameters on the Microstructure of TiC-Fe Multiphase and Multilayer Coatings, *Surf. Coat. Technol.*, 1992, **50**, p 233-239
106. I. Ozdemir, I. Hamanaka, M. Hirose, Y. Tsunekawa, and T.M. Okumiya, In Situ Formation of Al-Si-Mg Based Composite Coating by Different Reactive Thermal Spray Processes, *Surf. Coat. Technol.*, 2005, **200**, p 1155-1161
107. A.J. Allen, G.G. Long, H. Boukari, J. Ilavsky, A. Kulkarni, S. Sampath, H. Herman, and A.N. Goland, Microstructural Characterization Studies to Relate the Properties of Thermal Spray Coatings to Feedstock and Spray Conditions, *Surf. Coat. Technol.*, 2001, **146-147**, p 544-552
108. T. Streibl, A. Vaidya, M. Friis, V. Srinivasan, and S. Sampath, A Critical Assessment of Particle Temperature Distributions During Plasma Spraying: Experimental Results for YSZ, *Plasma Chem. Plasma Proc.*, 2006, **26**(1), p 73-102
109. W. Chi, S. Sampath, and H. Wang, Ambient and High-Temperature Thermal Conductivity of Thermal Sprayed Coatings, *J. Therm. Spray Technol.*, 2006, **15**(4), p 773-778
110. G. Bertrand, P. Bertrand, P. Roy, C. Rio, and R. Mevrel, Low Conductivity Plasma Sprayed Thermal Barrier Coating Using Hollow PSZ Spheres: Correlation Between Thermophysical Properties and Microstructure, *Surf. Coat. Technol.*, 2008, **202**, p 1994-2001
111. R. Cuenca Alvarez, H. Ageorges, P. Fauchais, P. Fournier, and A. Smith, The Effect of the Mechanofusion Process and Planetary Milling on Composite Powder Preparation: Agglomeration and Fragmentation, *Mater. Sci. Forum*, 2003, **442**, p 67-72
112. R. Cuenca-Alvarez, ''Contribution to the Elaboration of Composites Coatings by Mechanofused Powders Direct Current Plasma Sprayed,'' Ph.D. thesis, University of Limoges, France, 2003 (in French)
113. T. Stoltenhoff, H. Kreye, and H.J. Richter, An Analysis of the Cold Spray Process and Its Coatings, *J. Therm. Spray Technol.*, 2002, **11**(4), p 542-550
114. S.V. Klinkov and V.F. Kosarev, Measurements of Cold Spray Deposition Efficiency, *J. Therm. Spray Technol.*, 2006, **15**(3), p 364-371
115. C.-J. Li, W.-Y. Li, Y.-Y. Wang, G.-J. Yang, and H. Fukanuma, A Theoretical Model for Prediction of Deposition Efficiency in Cold Spraying, *Thin Sol. Films*, 2005, **489**, p 79-85
116. A.P. Alkhimov, S.V. Klinkov, and V.F. Kosarev, Study of Heat Exchange of Supersonic Plane Jet with Obstacle at Gas-Dynamic Spraying, *Thermophys. Aeromech.*, 2000, **7**(3), p 375-382
117. J.H. Lee, J.S. Kim, S.M. Shin, C.H. Lee, and H.J. Kim, Effect of Particle Temperature on the Critical Velocity for Particle Deposition by Kinetic Spraying, *Building on 100 Years of Success: Proceedings of the International Thermal Spray Conference 2006*, B.R. Marple, M.M. Hyland, Y.-C. Lau, R.S. Lima, and J. Voyer, Ed., ASM International, Materials Park, OH, USA, 2006, e-proceedings
118. H. Katanoda, M. Fukuhara, and N. Iino, Numerical Study of Combination Parameters for Particle Impact Velocity and Temperature in Cold Spray, *J. Therm. Spray Technol.*, 2007, **15**(5-6), p 627-633
119. H. Katanoda, M. Fukuhara, and N. Iino, Numerical Study of Combination Parameters for Particle Impact Velocity and Temperature in Cold Spray, *Thermal Spray 2007: Global Coating Solutions*, B.R. Marple, M.M. Hyland, Y.-C. Lau, C.-J. Li, R.S. Lima, and G. Montavon, Ed., ASM International, Materials Park, OH, USA, 2007, p 72-77
120. H. Mäkinen, J. Lagerbom, and P. Vuoristo, Adhesion of Cold Sprayed Coatings: Effect of Powder, Substrate, and Heat Treatment, *Thermal Spray 2007: Global Coating Solutions*, B.R. Marple, M.M. Hyland, Y.-C. Lau, C.-J. Li, R.S. Lima, and G. Montavon, Ed., ASM International, Materials Park, OH, USA, 2007, p 31-36
121. D. Helfritch and V. Champagne, Optimal Particle Size for the Cold Spray Process, *Building on 100 Years of Success: Proceedings of the International Thermal Spray Conference 2006*, B.R. Marple, M.M. Hyland, Y.-C. Lau, R.S. Lima, and J. Voyer Ed., ASM International, Materials Park, OH, USA, 2006, e-proceedings
122. R.C. Dykhuizen, M.F. Smith, D.L. Gilmore, R.A. Neiser, X. Jiang, and S. Sampath, Impact of High Velocity Cold Spray Particles, *J. Therm. Spray. Technol.*, 1999, **8**(4), p 559-564
123. K.C. Kang, S.H. Yoon, Y.G. Ji, and C. Lee, Oxidation Effects on the Critical Velocity of Pure Al Feedstock Deposition in the Kinetic Spraying Process, *Thermal Spray 2007: Global Coating Solutions*, B.R. Marple, M.M. Hyland, Y.-C. Lau, C.-J. Li, R.S. Lima, and G. Montavon, Ed., ASM International, Materials Park, OH, USA, 2007, p 66-71
124. L.L. Shaw, D. Goberman, R. Ren, M. Gell, S. Jiang, Y. Wang, T.D. Xiao, and P.R. Strutt, The Dependency of Microstructure and Properties of Nanostructured Coatings on Plasma Spray Conditions, *Surf. Coat. Technol.*, 2000, **130**, p 1-8
125. R.S. Lima and B.R. Marple, From APS to HVOF Spraying of Conventional and Nanostructured Titania Feedstock Powders: A Study on the Enhancement of the Mechanical Properties, *Surf. Coat. Technol.*, 2000, **200**, p 3428-3437
126. S.-O. Chwa, D. Klein, F.L. Toma, G. Bertrand, H. Liao, C. Coddet, and A. Ohmori, Microstructure and Mechanical Properties of Plasma Sprayed Nanostructured TiO_2-Al Composite Coatings, *Surf. Coat. Technol.*, 2005, **194**, p 215-224
127. E.P. Song, J. Ahn, S. Lee, and N.J. Kim, Microstructure and Wear Resistance of Nanostructured Al_2O_3-8wt% TiO_2 Coatings Plasma-Sprayed with Nanopowders, *Surf. Coat. Technol.*, 2006, **201**, p 1309-1315
128. P. Ctibor, K. Neufuss, and P. Chraska, Microstructure and Abrasion Resistance of Plasma Sprayed Titania Coatings, *J. Therm. Spray Technol.*, 2006, **15**(4), p 689-694
129. J. Ahn, B. Hwang, E.P. Song, S. Lee, and N.J. Kim, Correlation of Microstructure and Wear Resistance of Al_2O_3-TiO_2 Coatings Plasma Sprayed with Nanopowders, *Metal. Mater. Trans. A*, 2006, **37**, p 1851-1861
130. E.P. Song, J. Ahn, S. Lee, and N.J. Kim, Effects of Critical Plasma Spray Parameter and Spray Distance on Wear Resistance of Al_2O_3-8 wt.%TiO_2 Coatings Plasma-Sprayed with Nanopowders, *Surf. Coat. Technol.*, 2008, **202**, p 3625-3632
131. R.S. Lima, C. Moreau, and B.R. Marple, HVOF-Sprayed Coatings Engineered from Mixtures of Nanostructured and Submicron Al_2O_3-TiO_2 Powders: An Enhanced Wear Performance, *J. Therm. Spray Technol.*, 2007, **16**(5-6), p 866-872
132. T. Varis, J. Knuuttila, E. Turunen, J. Leivo, J. Silvonen, and M. Oksa, Improved Protection Properties by Using Nanostructured Ceramic Powders for HVOF Coatings, *J. Therm. Spray Technol.*, 2007, **16**(4), p 524-532
133. A. Ibrahim, R.S. Lima, C.C. Berndt, and B.R. Marple, Fatigue and Mechanical Properties of Nanostructured and Conventional Titania (TiO_2) Thermal Spray Coatings, *Surf. Coat. Technol.*, 2007, **201**, p 7589-7596
134. H. Chen, C. Ding, P. Zhang, P. La, and S.W. Lee, Wear of Plasma-Sprayed Nanostructured Zirconia Coatings Against Stainless Steel Under Distilled-Water Conditions, *Surf. Coat. Technol.*, 2003, **173**, p 144-149
135. S. Tao, B. Liang, C. Ding, H. Liao, and C. Coddet, Wear Characteristics of Plasma-Sprayed Nanostructured Yttria Partially Stabilized Zirconia Coatings, *J. Therm. Spray Technol.*, 2005, **14**(4), p 518-523
136. B.R. Marple and R.S. Lima, Process Temperature/Velocity-Hardness-Wear Relationships for High-Velocity Oxyfuel

Sprayed Nanostructured and Conventional Cermet Coatings, *J. Therm. Spray Technol.*, 2005, **14**(1), p 67-76
137. C. Bartuli, T. Valente, F. Cipri, E. Bemporad, and M. Tului, Parametric Study of an HVOF Process for the Deposition of Nanostructured WC-Co Coatings, *J. Therm. Spray Technol.*, 2005, **14**(2), p 187-195
138. J.M. Guilemany, S. Dosta, and J.R. Miguel, The Enhancement of the Properties of WC-Co HVOF Coatings Through the Use of Nanostructured and Microstructured Feedstock Powders, *Surf. Coat. Technol.*, 2006, **201**, p 1180-1190
139. S. Siegmann, O. Brandt, and M. Dvorak, Thermally Sprayed Wear Resistant Coatings with Nanostructured Hard Phases, *J. Therm. Spray Technol.*, 2004, **13**(1), p 37-43
140. S. Matthews, M. Hyland, and B. James, Long-Term Carbide Development in High-Velocity Oxygen Fuel/High-Velocity Air Fuel Cr_3C_2-NiCr Coatings Heat Treated at 900 °C, *J. Therm. Spray Technol.*, 2004, **13**(4), p 526-536
141. M. Roy, A. Pauschitz, J. Bernardi, T. Koch, and F. Franek, Microstructure and Mechanical Properties of HVOF Sprayed Nano-Crystalline Cr_3C_2-25(Ni20Cr) Coating, *J. Therm. Spray Technol.*, 2006, **15**(3), p 372-381
142. J. Gang, T. Grosdidier, and J.-P. Morniroli, Microstructure of a High-Velocity Oxy-Fuel Thermal-Sprayed Nanostructured Coating Obtained from Milled Powder, *Met. Mater. Trans. A*, 2007, **38**, p 2455-2463
143. E. Turunen, T. Varis, T.E. Gustafsson, J. Keskinen, T. Falt, and S.-P. Hannula, Parameter Optimization of HVOF Sprayed Nanostructured Alumina and Alumina-Nickel Composite Coatings, *Surf. Coat. Technol.*, 2006, **200**, p 4987-4994
144. C.-Q.Li, S. Ma, and X.L. Ye, Tribological Properties of Nanostructured n-Al_2O_3/Ni Coatings Deposited by Plasma Spraying, *J. Cent. South Univ. Technol.*, 2005, **12**(2), p 237-241
145. A.K. Basak, S. Achanta, J.-P. Celis, M. Vardavoulias, and P. Matteazzi, Structure and Mechanical Properties of Plasma Sprayed Nanostructured Alumina and FeCuAl-Alumina Cermet Coatings, *Surf. Coat. Technol.*, 2008, **202**, p 2368-2373
146. C. Hwang and C.-H. Yu, Formation of Nanostructured YSZ/Ni Anode with Pore Channels by Plasma Spraying, *Surf. Coat. Technol.*, 2007, **201**, p 5954-5959
147. L. Ajdelsztajn, F. Tang, G.E. Kim, V. Provenzano, and J.M. Schoenung, Synthesis and Oxidation Behavior of Nano-Crystalline MCrAlY Bond Coatings, *J. Therm. Spray Technol.*, 2005, **14**(1), p 23-30
148. F. Tang, L. Ajdelsztajn, G.E. Kim, V. Provenzano, and J.M. Schoenung, Effects of Surface Oxidation During HVOF Processing on the Primary Stage Oxidation of a CoNiCrAlY Coating, *Surf. Coat. Technol.*, 2004, **185**, p 228-233
149. F. Otsubo, H. Era, and K. Kishitake, Formation of Amorphous Fe-Cr-Mo-8P-2C Coatings by the High Velocity Oxy-Fuel Process, *J. Therm. Spray Technol.*, 2000, **9**(4), p 494-498
150. H. Choi, J. Kim, C. Lee, and K.-H. Lee, Critical Factors Affecting the Amorphous Phase Formation of NiTiZrSiSn Bulk Amorphous Feedstock in Vacuum Plasma Spray, *J. Mater. Sci.*, 2005, **40**, p 3873-3875
151. H. Choi, S. Lee, B. Kim, H. Jo, and C. Lee, Effect of In-Flight Particle Oxidation on the Phase Evolution of HVOF NiTiZrSiSn Bulk Amorphous Coating, *J. Mater. Sci.*, 2005, **40**, p 6121-6126
152. M. Parco, I. Fagoaga, K. Bobzin, E. Lugsheider, J. Zwick, and G. Hildago, Developement and Characterization of Nanostructured Iron-Based Coatings by HFPD and HVOF, *Building on 100 Years of Success: Proceedings of the International Thermal Spray Conference 2006*, B.R. Marple, M.M. Hyland, Y.-C. Lau, R.S. Lima, and J. Voyer, Ed., ASM International, Materials Park, OH, USA, 2006, e-proceedings
153. D.J. Branagan, M. Breitsameter, B.E. Meacham, and V. Belashchenko, High-Performance Nanoscale Composite Coatings for Boiler Applications, *J. Therm. Spray Technol.*, 2005, **14**(2), p 196-204
154. J. Wilden, J.P. Bergmann, S. Reich, S. Schlichting, Th. Schnick, Cladding of Aluminum Substrates with Nano Crystalline Solidifying Wear Resistant Iron-Based Materials, *Thermal Spray 2007: Global Coating Solutions*, B.R. Marple, M.M. Hyland, Y.-C. Lau, C.-J. Li, R.S. Lima, and G. Montavon, Ed., ASM International, Materials Park, OH, USA, 2007, p 1075-1079
155. V. Viswanathan, T. Laha, K. Balani, A. Agarwal, and S. Seal, Challenges and Advances in Nanocomposite Processing Techniques, *Mater. Sci. Eng.*, 2006, **R54**, p 121-285
156. L. Ajdelsztajn, A. Zúñiga, B. Jodoin, and E.J. Lavernia, Cold-Spray Processing of a Nano-Crystalline Al-Cu-Mg-Fe-Ni Alloy with Sc, *J. Therm. Spray Technol.*, 2006, **15**(2), p 184-190
157. H.-T. Wang, C.-J. Li, G.-J. Yang, C.-X. Li, Q. Zhang, and W.-Y. Li, Microstructural Characterization of Cold Sprayed Nanostructured FeAl Intermetallic Compound Coating and Its Ball-Milled Feedstock Powders, *J. Therm. Spray Technol.*, 2007, **16**(5-6), p 669-676
158. P. Richer, B. Jodoin, L. Ajdelsztajn, and E.J. Lavernia, Substrate Roughness and Thickness Effects on Cold Spray Nano-Crystalline Al-Mg Coatings, *J. Therm. Spray Technol.*, 2006, **15**(2), p 246-254
159. E. Sansoucy, G.E. Kim, A.L. Moran, and B. Jodoin, Mechanical Characteristics of Al-Co-Ce Coatings Produced by the Cold Spray Process, *J. Therm. Spray Technol.*, 2007, **16**(5-6), p 651-660
160. L. Ajdelsztajn, B. Jodoin, and J.M. Schoenung, Synthesis and Mechanical Properties of Nano-Crystalline Ni Coatings Produced by Cold Gas Dynamic Spraying, *Surf. Coat. Technol.*, 2006, **201**, p 1166-1172
161. Q. Zhang, C.-J. Li, C.-X. Li, G.-J. Yang, and S.-C. Lui, Study of Oxidation Behavior of Nanostructured NiCrAlY Bond Coatings Deposited by Cold Spraying, *Surf. Coat. Technol.*, 2008, **202**, p 3378-3384
162. C.-J. Li, G.-J. Yang, P.-H. Gao, J. Ma, Y.-Y. Wang, and C.-X. Li, Characterization of Nanostructured WC-Co Deposited by Cold Spraying, *J. Therm. Spray Technol.*, 2007, **16**(5-6), p 1011-1020
163. P. Fauchais, V. Rat, C. Delbos, J.-F. Coudert, T. Chartier, and L. Bianchi, Understanding of Suspension dc Plasma Spraying of Finely Structured Coatings for SOFC, *IEEE Trans. Plasma Sci.*, 2005, **33**(2), p 920-930
164. J. Fazilleau, C. Delbos, V. Rat, J.-F. Coudert, P. Fauchais, and B. Pateyron, Phenomena Involved in Suspension Plasma Spraying. Part 1: Suspension Injection and Behaviour, *Plasma Chem. Plasma Proc.*, 2006, **26**(4), p 371-391
165. J. Oberste-Berghaus, B. Marple, and C. Moreau, Suspension Plasma Spraying of Nanostructured WC-12Co Coatings, *J. Therm. Spray Technol.*, 2006, **15**(4), p 676-681
166. R. Gadow, A. Killinger, and J. Rauch, New Results in High Velocity Suspension Flame Spraying (HVSFS), *Surf. Coat. Technol.*, 2008, **202**, p 4329-4336